JAERI-M
83-076

PROGRESS REPORT ON SAFETY RESEARCH OF HIGH-LEVEL WASTE MANAGEMENT FOR THE PERIOD APRIL, 1982 TO MARCH 1983

June 1983

(Ed.) Haruto NAKAMURA and Shingo TASHIRO

日本原子力研究所
Japan Atomic Energy Research Institute

JAERI-M レポートは，日本原子力研究所が不定期に公刊している研究報告書です。
入手の問合わせは，日本原子力研究所技術情報部情報資料課（〒319—11 茨城県那珂郡東海村）あて，お申しこしください。なお，このほかに財団法人原子力弘済会資料センター（〒319—11 茨城県那珂郡東海村日本原子力研究所内）で複写による実費頒布をおこなっております。

JAERI-M reports are issued irregularly.
Inquiries about availability of the reports should be addressed to Information Section, Division of Technical Information, Japan Atomic Energy Research Institute, Tokai-mura, Naka-gun, Ibaraki-ken 319—11, Japan.

編集兼発行　日本原子力研究所
印　　刷　日立高速印刷株式会社

JAERI-M 83-076

Progress Report on Safety Research of High-Level Waste Management for The Period April, 1982 to March, 1983

(Ed.) Haruto NAKAMURA and Shingo TASHIRO
Department of Environmental Safety Research,
Tokai Research Establishment, JAERI

(Received April 28, 1983)

Main results obtained on Safety Research of High-Level waste Management in 1982 were editted.

1) The leaching mechanisms of the vitrified waste were studied to estimate the leach rate in disposal condition.
2) For the safety assessment of storage and disposal of the returning waste resulted from overseas reprocessing, properties of the glass simulating the composition by COGEMA are being measured.
3) In order to assess the integrity of the repository, influence of heat on the characteristics of rock mass and buffer materials was studied in underground drift. And also the retardation mechanism of the leached elements by rock mass was discussed.
4) The construction of Waste Safety Testing Facility (WASTEF) was completed, and vitrification test and near-field test using large radiation sources were initiated.

Keyword: High-level Waste, Glass Form, Characterization, WASTEF Storage Facility, Geological Disposal, Safety Assessment, Progress Report, Leaching Mechanism, Retardation.

JAERI－M 83－076

高レベル廃棄物処理処分に関する研究報告
（昭和57年４月～昭和58年３月）

日本原子力研究所東海研究所環境安全研究部
（編）中村　治人・田代　晋吾

（1983年４月28日受理）

57年度に行った高レベル廃棄物処理処分に関する安全性研究の主な成果を収録した。

1） 処分環境での浸出率を評価するため，ガラス固化体の浸出機構を検討した。

2） 海外再処理に伴い発生する返還廃棄物の貯蔵及び処分の安全評価のため，COGEMA組成の模擬ガラス固化体の特性試験を行った。

3） 地層処分の安全評価のため，地下坑道内で岩盤及び埋戻し材の加熱特性試験を行った。また，岩盤による浸出成分の移行遅延機構について検討した。

4） 廃棄物安全試験施設の建設を完了し，ガラス固化試験及び大線源を使ったニヤフィールド試験を開始した。

Contents

Introduction

H. Nakamura

The revised national program for high-level waste (HLW) management that HLW should be vitrified, stored for appropriate term and transfered to the repository in deep underground was shown by the Japan Atomic Energy Commission in 1980. Research and development of new technologies, such as ceramic solidification and partitioning process, are also required.

The Japan Atomic Energy Research Institute (JAERI) plays a role in the safety studies and research on technologies according to the national program. This report reviews main results obtained in the last fiscal year of 1982 following the progress report of 1981.

Topics in each field are following;

The leaching mechanisms of the vitrified waste were studied to estimate the leach rate in disposal condition. The formation of sheet silicate crystal was identified in gel layer on leached glass, which was liable to retard the migration. Leachability was reduced by covering the glass with grain of rock and glass. This result suggests low leachability of glass buried in rock and usability of glass powder as a component of the buffer material.

For the safety assessment of storage and disposal of the returning waste resulted from overseas reprocessing, properties of the glass simulating the composition by COGEMA in France are being measured on consignment of Japanese Electric Power Companies.

To suport the regulatory authority, inspection methodology of storage facility are being developed on technical point of view and calculation codes for safety assessment were also investigated.

Near-field test has been initiated to assess the compatibility of barrier materials under radiation and heat by using large radiation sources and spent fuels of JMTR.

Influence of heat on integrity of the repository was studied by heating rock mass and buffer materials buried in a drift at - 380 m from the ground surface. Number of fracture was increased by heating but restored the original state after cooling.

In order to clarify the retardation mechanism by rock mass, distribution coefficient of ^{137}Cs for mineral in fractures was compared with that to the grain of fresh rock and the large difference was confirmed. Reaction of leached elements with rock was studied at high temperature in an autoclave

to accelerate reactions.

The construction of Waste Safety Testing Facility (WASTEF) was completed and the operation tests of vitrification using trace amount of ^{137}Cs were carried out from November 1982 and near-field test using large radiation source of ^{90}Sr and ^{137}Cs was initiated.

The main subjects in 1983 will be the operation of WASTEF using large amount of radioactive materials and construction of a new underground research facility in granitic rock mass.

1. Glass waste form examination

1.1 Leachability of the glass waste form covered with rock and glass powder

T. BANBA

Considering the leachability of glass waste form after disposal in rock formation, it is necessary to take account of the influence of surrounding materials such as buffer materials and rock formations. The simulated waste glass covered with rock or glass-frit powder was investigated in its leachability to clarify the leaching mechanism in the disposal conditions.

Experimental

The glass waste form used for this experiment was a borosilicate glass with 11.7 wt% simulated waste oxides, which has the composition shown in Table 1. Fig. 1 shows a leach test apparatus. Cylindrical specimens ($5\ mm^{\phi} \times 5\ mm^{H}$) were leached at 100°C for 1 day to 10 days using teflon vessel which contained (1) only 15 ml of deionized water, (2) glass-frit powder and water, (3) granite powder and water and (4) basalt powder and water. The glasses were covered with the powders of about 4 gram in size of between 0.25 mm and 0.50 mm. The composition of the glass frit is given in Table 2, and granite and basalt were received from Inada-machi, Ibaragi-ken and Iwafuma-machi, Tochigi-ken, respectively. The leaching solutions were analyzed by means of inductively coupled plasma atomic emission spectroscopy(ICP) and flame atomic absorption spectroscopy.

Results and discussion

Fig. 2 shows the fractional weight loss as a function of time at 100°C. The weight loss of waste glass decreased by covering it with the powder, especially, glass-frit powder. The weight loss of waste glass in glass-frit powder- water is hardly dependent on leached time and is smaller than tenth of the weight loss in only water after 10 days. It is presumed that the solution is saturated with component of glass earlier than the rocks. Basalt has a little effect on the decrease of weight loss.

Fig. 3 and Fig. 4 show the fractional releases of Cs and Sr to water at various time. As regards Cs, the differences between in only water and the others are very clear and the fractional releases to water become very little by coexistence of the powder of rocks and glass. Nevertheless

the weight loss of waste glass in basalt-water is larger than that in granite-water, the relation is opposite for the fractional release of Cs. The reason must be that leached Cs is absorbed on basalt more strongly than on granite. This result is consistent with the results of the experiment using mixture of rock and waste glass powder by Amemiya.(1)

As for the release of Sr, the differences between four cases are small, compared to the data of weight loss and Cs release. This result means that the rock and glass powder have little influence on the release of Sr to water, because Sr is absorbed by the powders and/or their hydrated products.

From our experiments, it is found that coexistence of the rocks and glass reduce the leachability of glass waste form, especially, glass-frit powder. This means that the leach rate in the rock will be small and glass-frit powder must be good protecter for leaching of the waste. Therefore, glass-frit powder can be used for the buffer material or its constituent.

Reference

(1) K. Amemiya, etal; 1983 Annual Meeting of the Atomic Energy Society of Japan (1983)

Table 1 Composition of glass waste form

component	weight-%	component	weight-%
SiO_2	48.49	NiO	0.326
B_2O_3	18.58	TeO_2	0.228
Al_2O_3	2.00	Cs_2O	0.980
Li_2O	1.865	BaO	0.626
Na_2O	11.30	La_2O_3	0.509
CaO	1.865	CeO_2	1.421
Rb_2O	0.122	Pr_6O_{11}	0.496
SrO	0.34	Nd_2O_3	1.654
Y_2O_3	0.201	Sm_2O_3	0.328
ZrO_2	1.647	Ag_2O	0.029
MoO_3	1.739	CdO	0.031
MnO_2	0.259	SnO_2	0.019
Fe_2O_3	0.587	Sb_2O_3	0.004
CoO	0.119	Gd_2O_3	0.038

Table 2 Recipe of glass frit

component	weight-%
SiO_2	62.38
B_2O_3	23.60
Al_2O_3	0.26
Li_2O	2.36
Na_2O	8.82
CaO	2.44

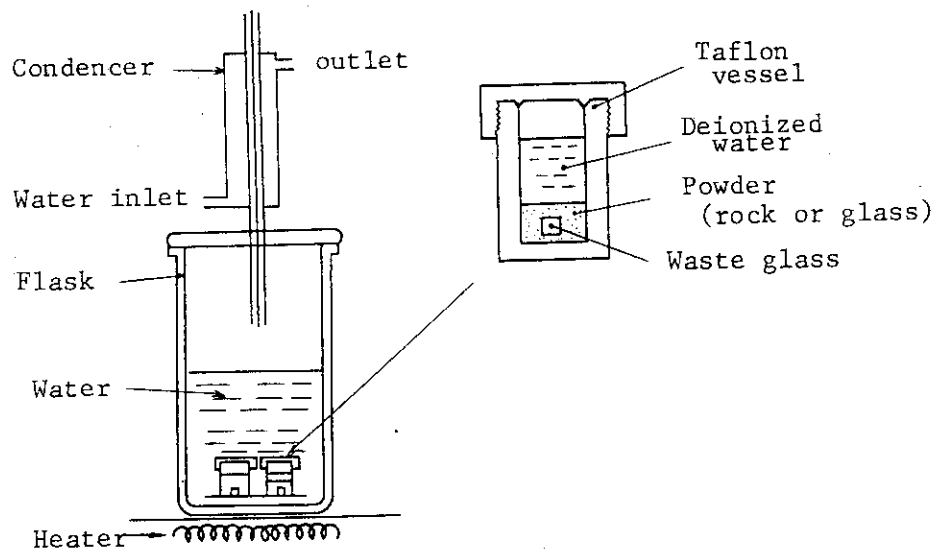

Fig. 1 Leach Test Apparatus

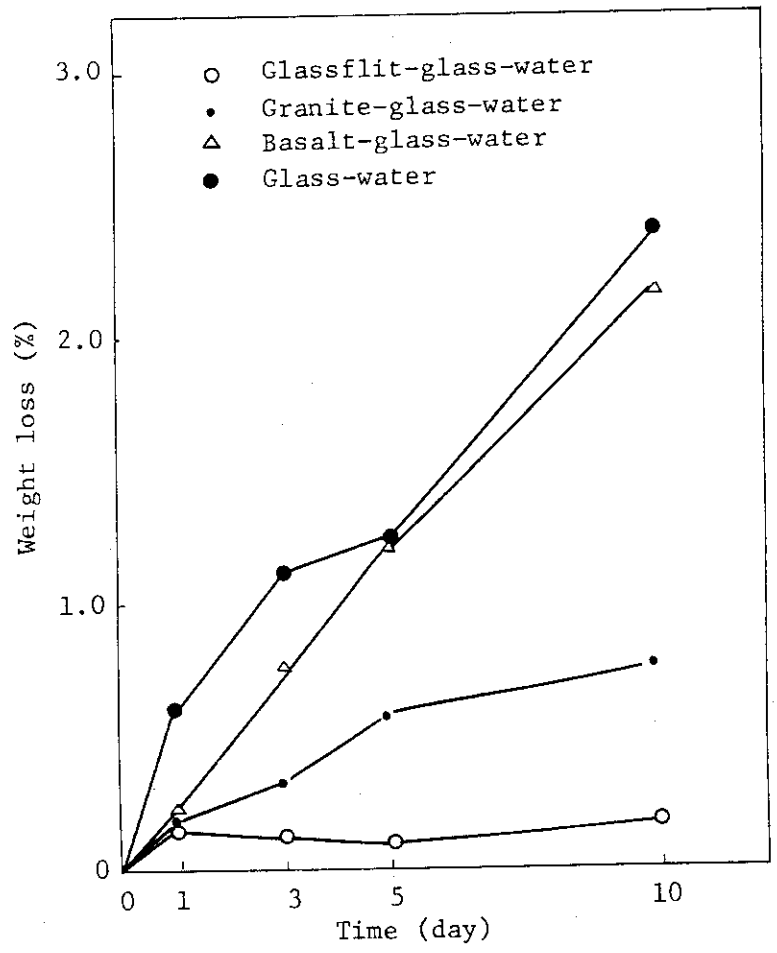

Fig. 2 Time dependence of fractional releases based on weight loss at 100°C

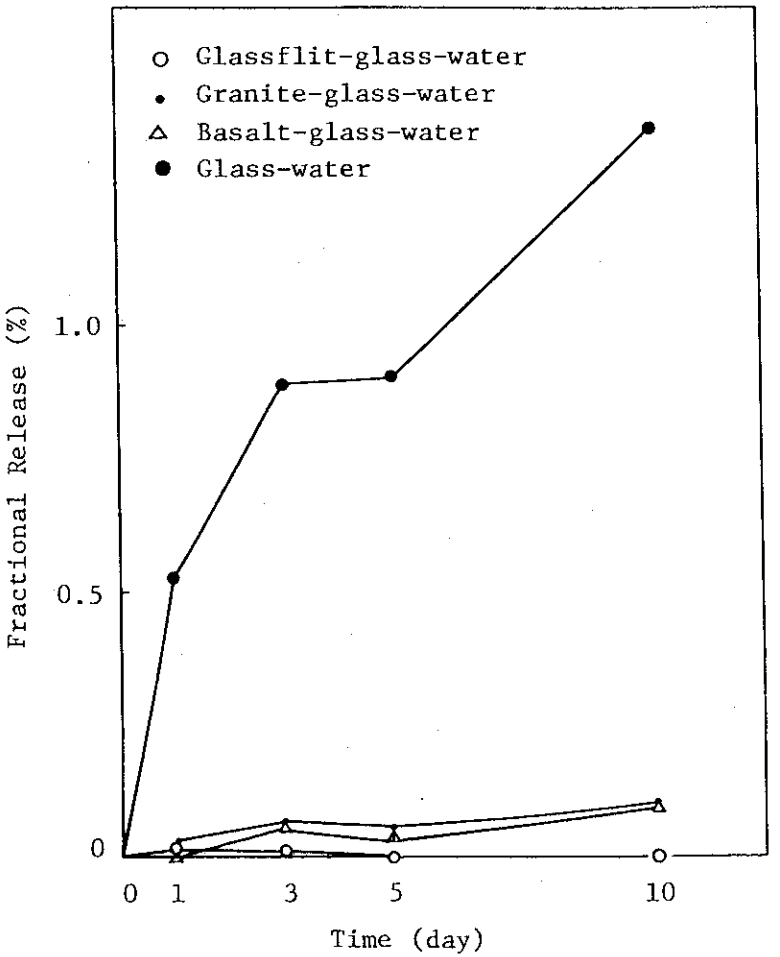

Fig. 3 Time dependence of fractional releases through water based on Cs at 100°C

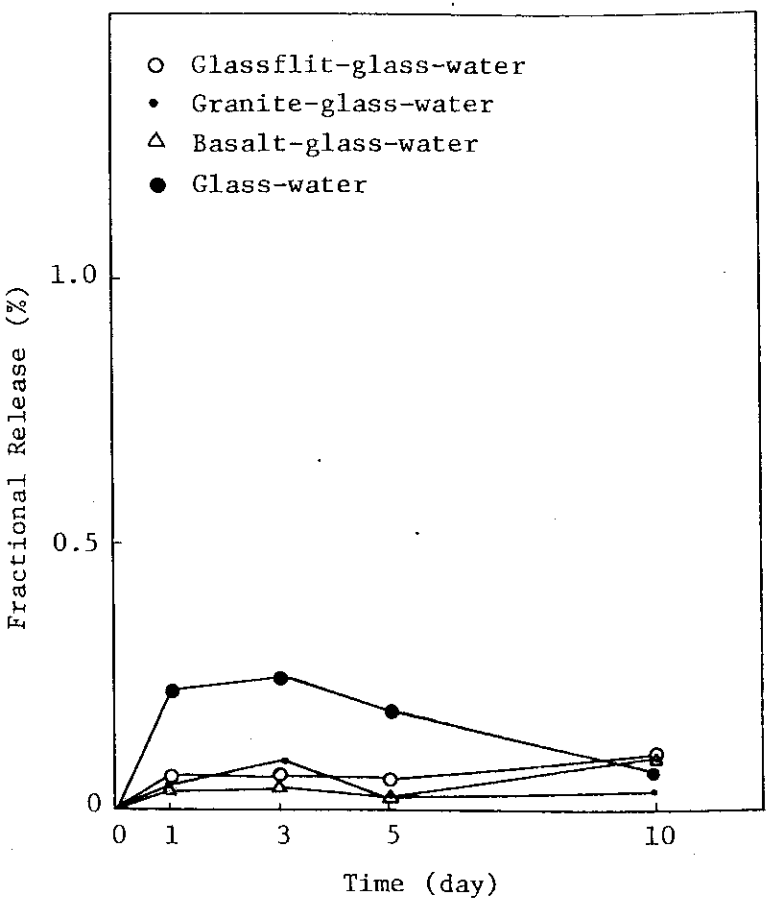

Fig. 4 Time dependence of fractional releases through water based on Sr at 100°C

1.2 Crystalline phase in surface layers of glass waste form

T. Murakami and T. Banba

Surface layers usually form on glass waste forms during leaching and they have a great influence on leach rate of radionuclides[1],[2]. One factor which complicates the leaching mechanisms is a kind of solid-liquid and/or solid-solid interactions in the surface layers, namely, precipitation or mineralization[3]. Since different radionuclides may stay in the surface layers in accordance with the formation of different crystalline phases, it is of considerable importance to confirm which crystalline phases form in the surface layers during leaching. Although the crystalline phases in the surface layers of glass waste forms have been examined[4],[5], their complete identification has not been carried out. The present paper gives the results of the examination of a crystalline phase in the surface layers of a glass waste form by means of analytical electron microscopy.

Experimental

The glass waste form used for this study was a borosilicate glass and contained 14 wt% nonradioactive simulated waste oxides[6]. The composition of the glass waste form is given in Table 1. After melting at 1200°C for two hours and then cooling, the glass waste form was cut into a block specimen of 7.3 × 6.5 × 4.5 mm in size. Soxleht leach test was carried out with the block specimen at 100°C for 200 days. The surface layers which formed on the glass waste form (Fig. 1) were ground to powder. The powdered specimens were finally subjected to analytical electron microscopy. Note that the surface layers were so fragile that they were broken easily by picking with a needle.

Results and discussion

A transmission electron microphotograph in Fig. 2(A) shows the aggregates of the crystalline phase which formed in the surface layers. Very small crystalline particles of around 100 to 1000 Å assemble together to make the botryoidal aggregates. More than 50 areas of the specimens were examined and they had a similar texture as that in Fig. 2(A) except one which showed growth of a crystal of around 3 μ (Fig. 3(A)).

Figure 2(B) shows the electron diffraction pattern of the selected area as shown by a circle in Fig. 2(A). The electron diffraction patterns of the specimens examined sometimes consisted of obvious diffraction spots and powder rings like the pattern in Fig. 2(B), and sometimes consisted of

powder rings alone. Comparison of the d spacings of the diffraction spots with those of the powder rings revealed these crystals belonged to the same crystalline phase. By rotating and tilting, the patterns of the diffraction spots were found to be essentially same as that in Fig. 3(B) which shows the diffraction pattern of the selected area as shown by a circle in Fig. 3(A). This means that there exists only one kind of crystalline phase or one kind of mineral group in the surface layers. Accordingly, we only need to analyze the pattern in Fig. 3(B) for identification of the crystalline phase which appeared in the surface layers.

The diffraction pattern in Fig. 3(B) has the following crystallographic features: (1) The angle between a^* and b^* axes is 90° and $a^* \neq b^*$ when a^* and b^* axes are assumed as shown in Fig. 3(B). (2) Extinction law, $h + k = 2n$, occurs. (3) A mirror plane normal to a^* and another mirror plane normal to b^* appear. (4) Moreover, Fig. 3(B) shows local symmetry of hexagonal rotation axes. (1), (2) and (3) indicate that the crystal system which has the above characteristics of the reciprocal lattice is orthrhombic system[7]. Around 50 specimens were examined on the basis of the above crystallographic characteristics and their cell dimensions varied from one specimen to another; a = 4.8 - 5.2 Å and b = 8.4 - 9.1 Å. No correction was made for the camera length of the transmission electron microscope. The c periodicity can not be determined at the present time but further investigations are now carried out.

Figure 4 gives the typical result of the elemental analysis of the crystalline phase by means of analytical electron microscopy. This phase was rich in Si and Fe and also contained Mg, Al, Zr, Mo, Ca, Ba, La, Ce, Nd and Ni.

The crystalline phase which formed in the surface layers of the glass waste form is found to be a sheet silicate[8] due to the following experimental results: (1) The phase is rich in Si and this implies the phase must be a silicate. (2) The phase has orthorhombic system and the cell dimensions; a = 4.8 - 5.2 Å and b = 8.4 - 9.1 Å and a and b have the relation, $b \doteqdot \sqrt{3} \cdot a$. (3) The phase has local symmetry of hexagonal rotation axes.

References

(1) Hench, L.L., Clark, D.E., Yen-Bower, E.L. : Nucl. Chem. Waste Manag., 1, 59 (1980).

(2) Kenna, B.T. : Nucl. Chem. Waste Manag., 3, 69, (1982).

(3) McVay, G.L., Buckwalter, C.R. : Nucl. Tech., 51, 123 (1980).

(4) Grambow, B. : In Scientific Basis for Nuclear Waste Management V, W. Lutze (Ed.), North-Holland, New York, 93 (1982).

(5) Strachan, D.M. : In Scientific Basis for Nuclear Waste Management V, W. Lutze (Ed.), North-Holland, New York, 181 (1982).

(6) Banba, T., Kimura, H., Kamizono, H., Tashiro, S. : JAERI-M 82-088, Japan Atomic Energy Research Institute, Tokai, Ibaraki (1982).

(7) Henry, N.F.M., Lonsdale, K. (Eds.) : International Tables for X-ray Crystallography vol. I, Kynoch Press, Birmingham, England (1952).

(8) Bragg, L., Claringbull, G.F. : Crystal Structures of Minerals, G. Bell and Sons Ltd., London (1965).

Table 1 Composition of glass waste form

Oxide form	Calculated (wt%)	Analytical (wt%)	Oxide form	Calculated (wt%)	Analytical (wt%)
SiO_2	38.3	—*	CoO	0.09	0.09
B_2O_3	13.0	11.8	NiO	0.50	0.42
Al_2O_3	3.52	7.38	Ag_2O	0.02	—
Na_2O	21.3	20.3	CdO	0.02	—
K_2O	1.14	—	TeO_2	0.17	—
MgO	1.49	0.84	Cs_2O	0.74	0.72
CaO	6.60	6.43	Ce_2O_3	1.13	—
SrO	0.25	0.24	Nd_2O_3	0.73	—
BaO	0.47	0.48	La_2O_3	0.35	—
TiO_2	0.06	0.09	Sm_2O_3	0.31	0.30
P_2O_5	1.32	0.25	Y_2O_3	0.29	0.25
Fe_2O_3	4.33	4.13	Pr_2O_3	0.17	—
MnO_2	0.24	0.22	Dy_2O_3	0.15	0.16
ZrO_2	1.24	1.05	Tb_2O_3	0.04	—
Rb_2O	0.10	—	Er_2O_3	0.03	—
MoO_3	1.31	1.37	Gd_2O_3	0.31	—
Cr_2O_3	0.29	0.20			

* Bars represent oxides which were not analyzed.

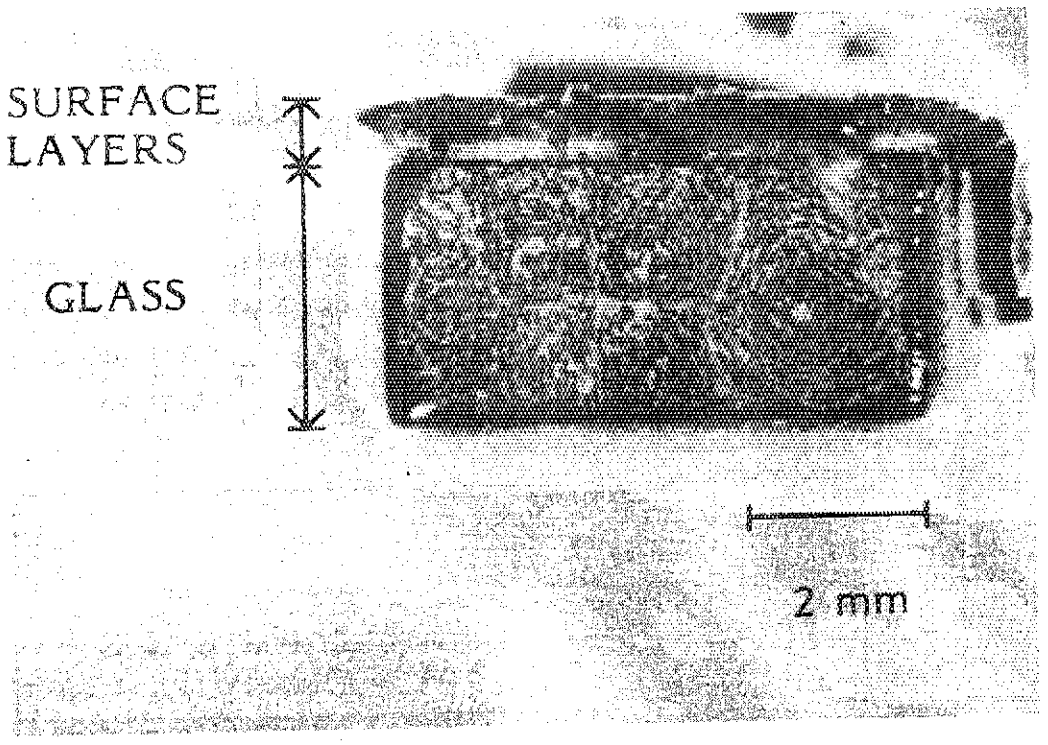

Fig. 1 Optical microphotograph of surface layers and galss waste form after leaching at 100°C for 200 days. Portion of the surface layers is shown.

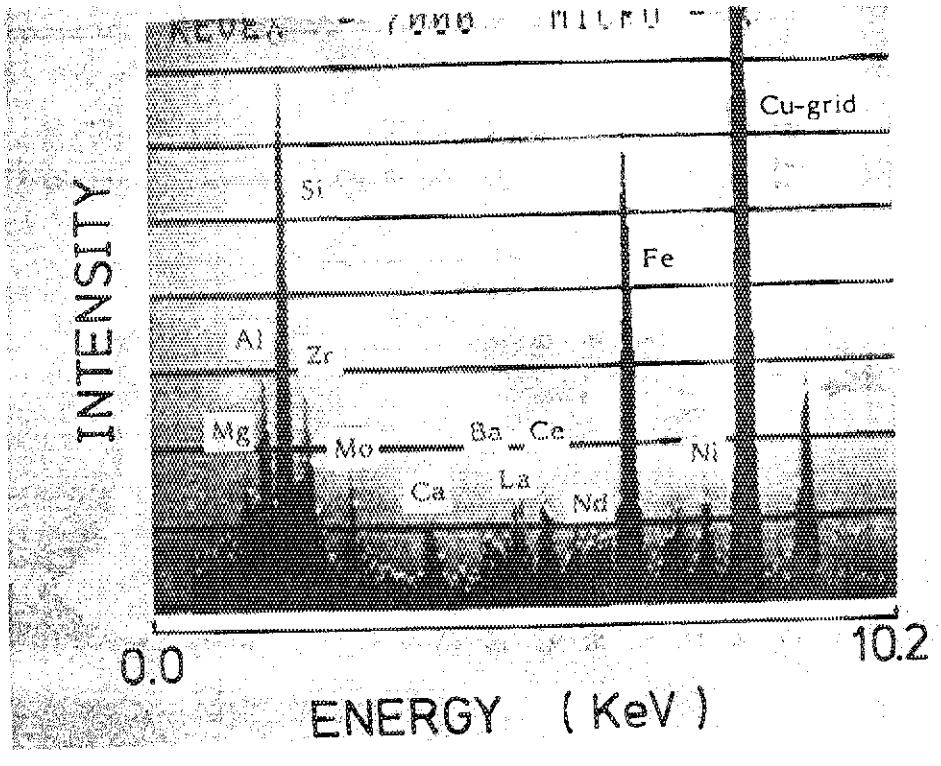

Fig. 4 Energy spectrum of sheet silicate in surface layers. Besides Si and Fe cations, large cations such as Ca, La, Ce, Nd also occur.

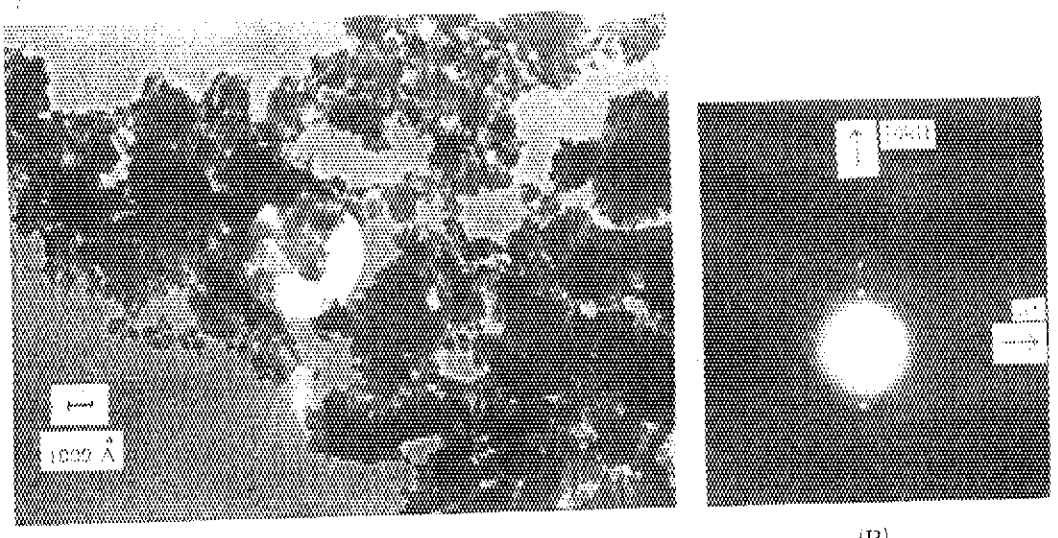

(A) (B)

Fig. 2 (A) Transmission electron microphotograph of powdered specimen of surface layers. Very small crystalline particles assemble together to make botryoidal aggregates. (B) Electron diffraction pattern of selected area shown by a circle in (A). Incomplete diffraction spots are accompanied by powder rings. The diffraction spots indicate there occur more than two crystals. Arrows show crystallographic axes.

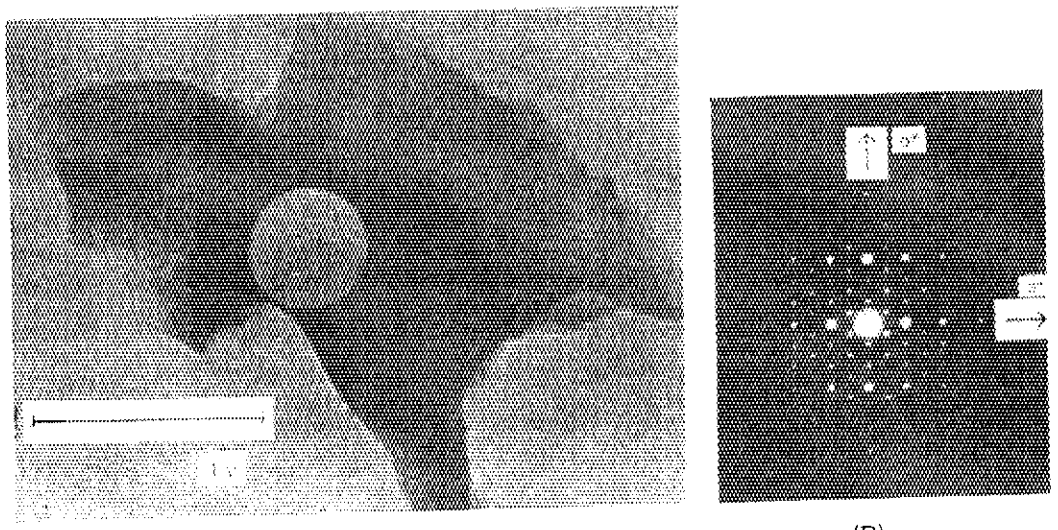

(A) (B)

Fig. 3 (A) Transmission electron microphotograph of largely grown crystal in surface layers. (B) Electron diffraction pattern of selected area shown by a circle in (A). Local symmetry of hexagonal rotation axes appears owing to the two-dimensional hexagonal network of the linked tetrahedra of the sheet silicate. Arrows show crystallographic axes.

1.3 Devitrification of a simulated high-level waste glass containing the elements of platinum group

H. Mitamura

High-level radioactive waste (HLW) contains the elements of platinum group which are hardly soluble in borosilicate glasses developed to vitrify the HLW[1]. Segregated materials of the platinum group elements in the glasses are liable to help the devitrification of the HLW glasses. In a previous report,[2] this phenomenon was examined by optical microphotography and constituents of a typical crystalline growing in a reference glass, which did not contain the platinum group elements, were determined. In the present paper, constituents of segregated materials and crystallines growing in a simulated HLW glass, which contained the platinum group elements, were determined.

Experiment

A simulated HLW glass containing 20 wt% waste oxides was used[2]. The glass was melted at 1200°C for 2 hours in an alumina crucible and annealed at 700°C for 1000 hours in an electric furnace in air in order to accelerate the devitrification.

The devitrified simulated HLW glass was subjected to an electron probe microanalyzer (X-650) using KEVEX analytical system.

Results

1. Areas where are rich in segregated materials of platinum group elements

Figure 1 and 2 show a backscattered electron image and an X-ray mapping image of ruthenium, respectively, for an area in the devitrified simulated HLW glass. Materials like leaves of a Japanese cedar in Fig. 1 were rich in ruthenium as shown in Fig. 2. Elemental analysis indicated that these materials consisted mainly of ruthenium. These materials were probably created as the result of recrystallization, because ruthenium-rich materials like such a shape could not be found before the annealing.

Figure 3 and 4 show a backscattered electron image and an X-ray mapping image of palladium, respectively, for another area in the devitrified simulated HLW glass. Large round materials in Fig. 3 were rich in palladium as shown in Fig. 4. The results of elemental analysis as shown in Fig. 5 indicated that palladium-rich materials consisted of palladium,

rhodium and tellurium. Constituents of segregated materials of platinum group elements in the devitrified simulated HLW glass were as same as those in an as-prepared simulated HLW glass[1].

2. Area where is poor in segregated materials of platinum group elements

Figure 6 shows a backscattered electron image for a devitrified area in the simulated HLW glass. Figure 7 indicates the result of elemental analysis for the crystalline as shown by an arrow of (a). This crystalline consisted mainly of silicon and rare earth elements. Elemental analysis for the cross-shape crystalline as shown by an arrow of (b) gave an energy spectrum similar to that in Fig. 7. Figure 8 shows the result of elemental analysis for the crystalline as shown by an arrow of (c). It is found in Fig. 8 that this crystalline consisted mainly of silicon, chromium, iron and nickel.

Comparison of the results of elemental analysis with those of X-ray diffractometry will be carried out in order to identify the crystallines growing in the devitrified simulated HLW glass.

References

1) H. Mitamura, T. Murakami, T. Banba, Y. Kiriyama, H. Kamizono, M. Kumata and S. Tashiro, "Segregation of the elements of platinum group in a simulated high-level waste glass", Nuclear and Chemical Waste Management (1983) (in press).

2) Progress Report on Safety Research of High-Level Waste Management for the Period April, 1981 to May, 1982, S. Tashiro (ed.), JAERI-M 82-145 (1982).

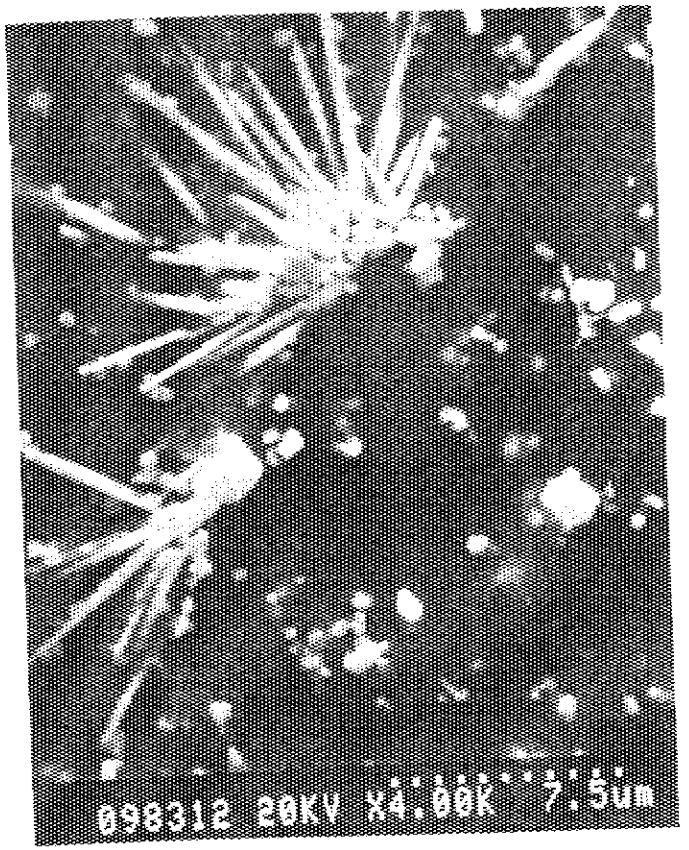

Fig. 1 Backscattered electron image for an area in the devitrified simulated HLW glass

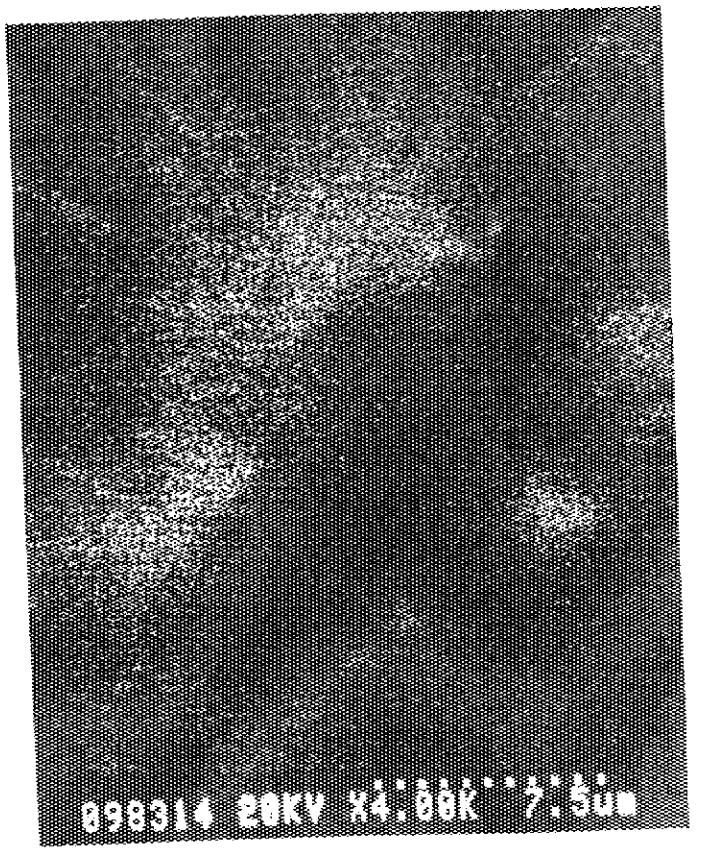

Fig. 2 X-ray mapping image of ruthenium for the area in Fig. 1

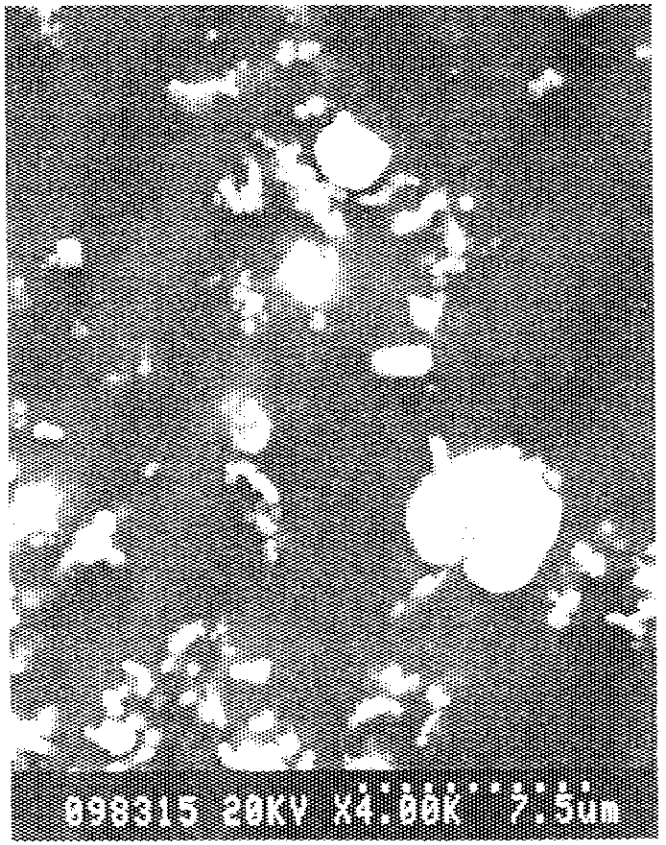

Fig. 3 Backscattered electron image for an area in the devitrified simulated HLW glass

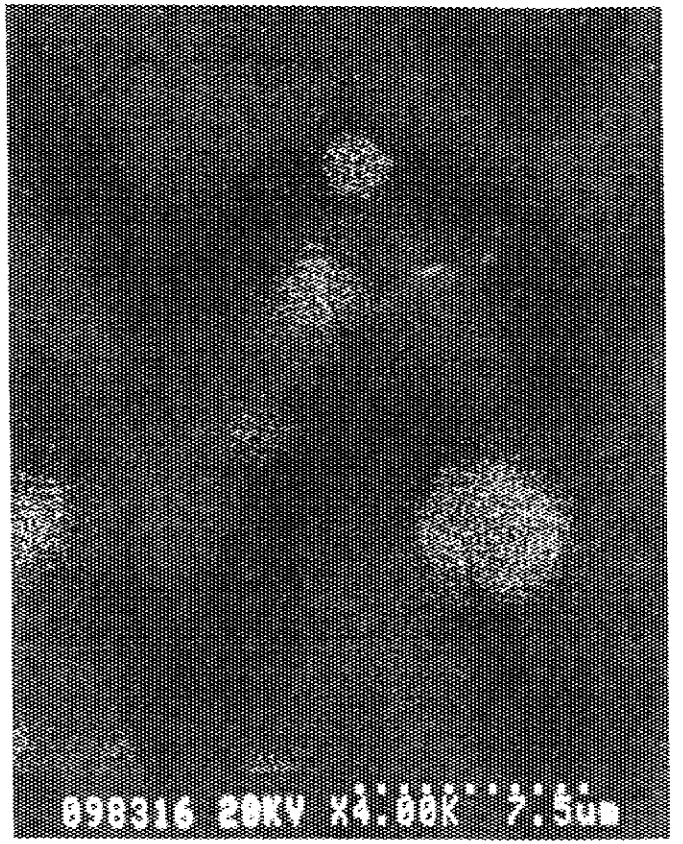

Fig. 4 X-ray mapping image of palladium for the area in Fig. 3

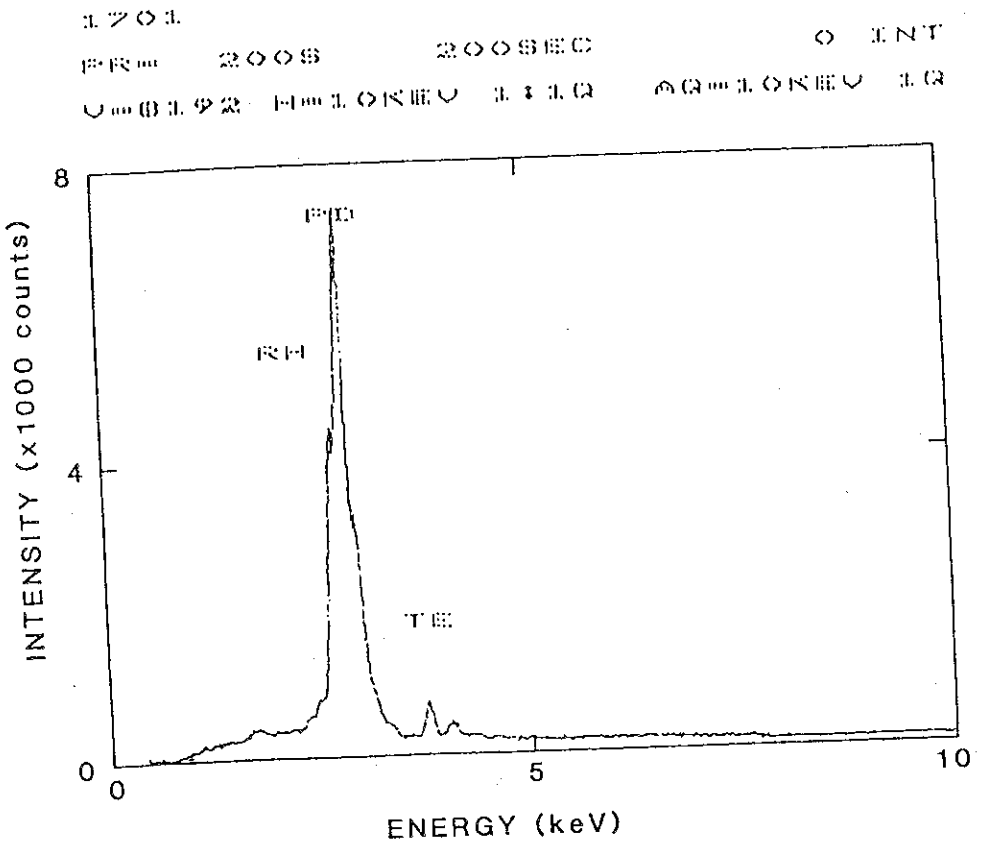

Fig. 5 Energy spectrum of a palladium-rich material with energy dispersive X-ray analysis

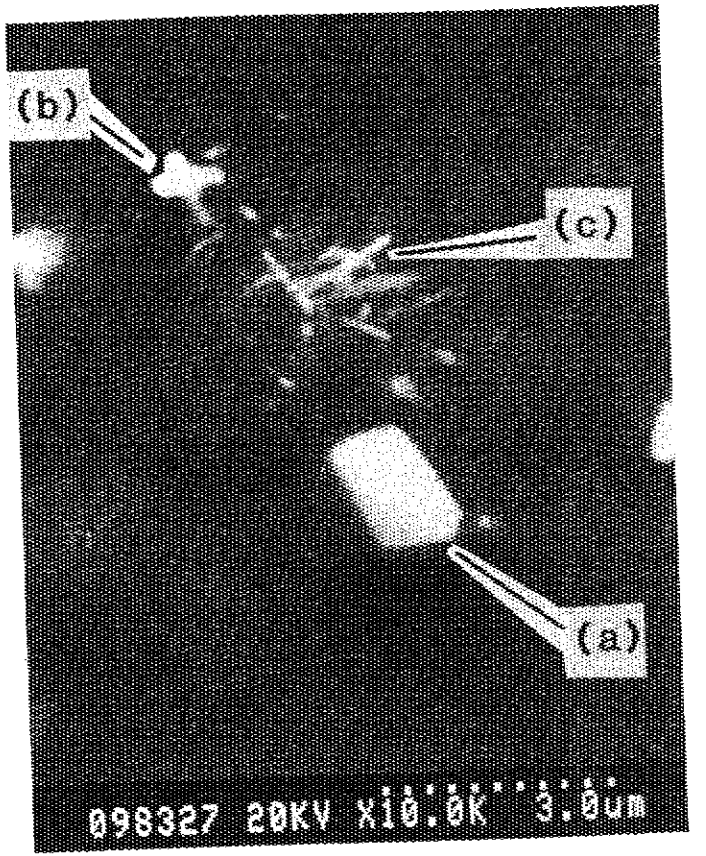

Fig. 6 Backscattered electron image for a devitrified area in the simulated HLW glass

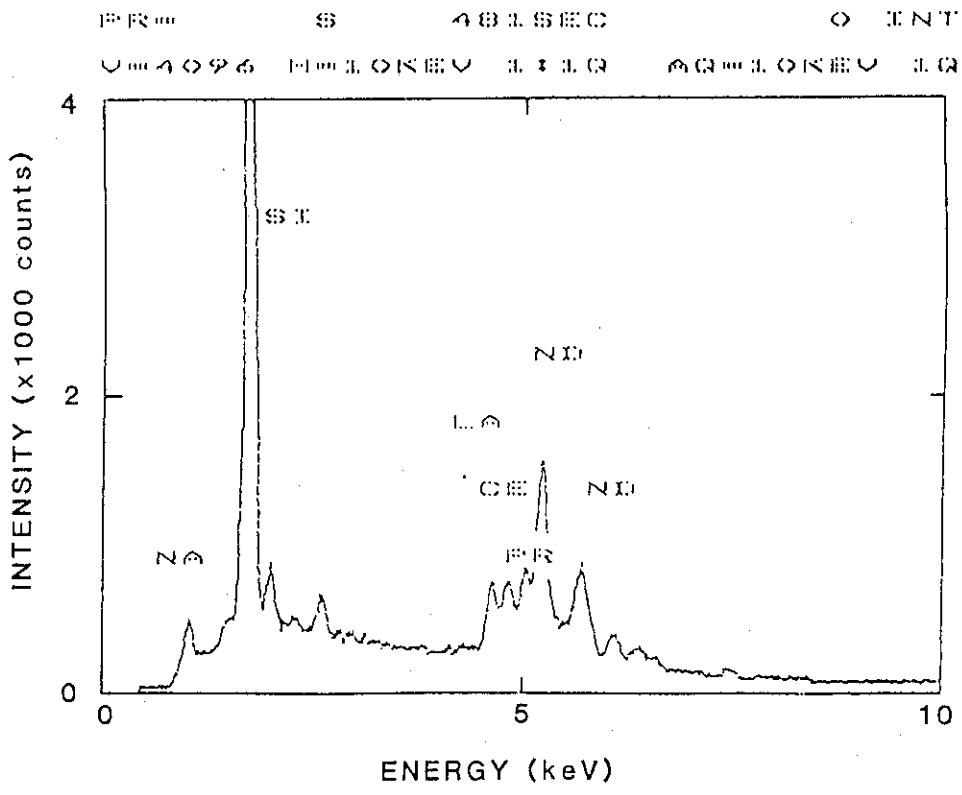

Fig. 7 Energy spectrum of a crystalline as shown by an arrow of (a) in Fig. 6 with energy dispersive X-ray analysis

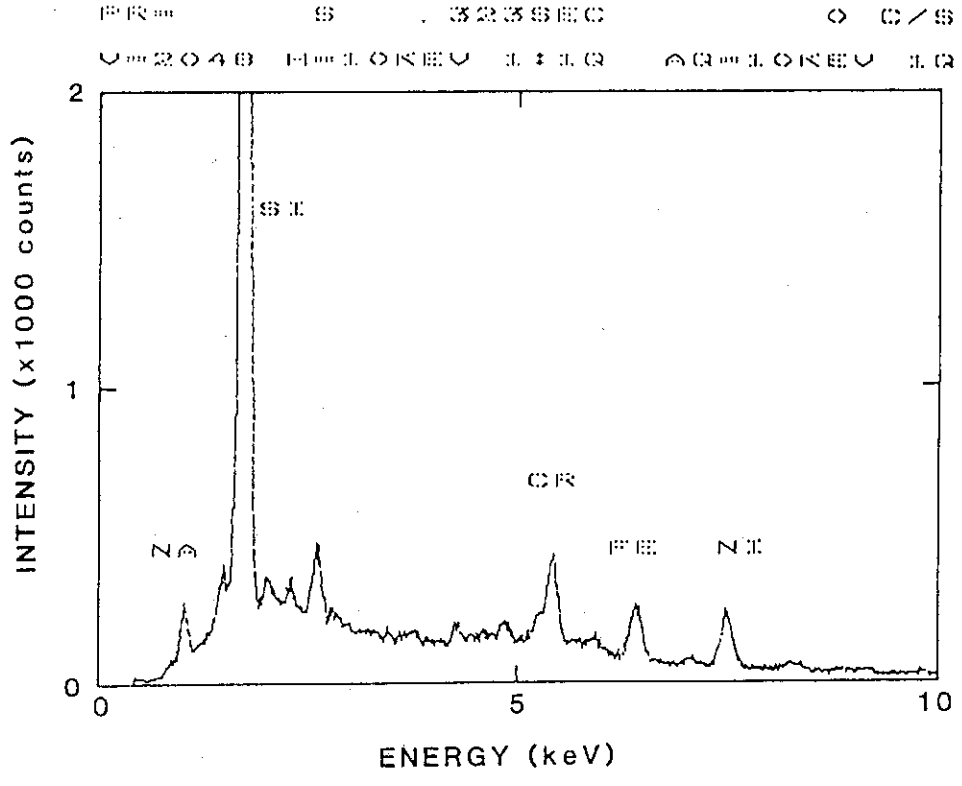

Fig. 8 Energy spectrum of a crystalline as shown by an arrow of (c) in Fig. 6 with energy dispersive X-ray analysis

1.4 Thermal shock resistance of vitrified products

H. Kamizono

Thermal shock of vitrified products may occur in case of decontamination of canisters by water or accidental fire fighting in a facility. Owing to such thermal shock, cracks will be created on the surface of vitrified products and the total surface area of vitrified products will be increased. The increase of the surface area may result in the increase of the fractional release of radioactive elements by leaching and in the decrease of mechanical strength. Such a change of chemical and physical properties of vitrified products has an influence on the safety of the storage and disposal of vitrified products. The object of this work is to clarify the thermal shock behavior of vitrified products.

Experimental

The sample used was a borosilicate glass containing 14% of simulated high level waste. The cylindrical specimen having a height of 25 mm and a diameter of 25 mm was heated at an elevated temperature for about 2 hrs and then dropped into water at room temperature. The temperature difference between the specimen and water was varied from 25 °C to 600°C. The surface area of cracks on the surface of quenched specimens was measured by a stereological linear intercept method. Static leach tests of the quenched specimens were conducted in deionized water at 100°C for 1 h. The bending strength, Young's modulus, and the thermal expansion coefficient of the specimen before quenching were measured in order to estimate the temperature difference above which surface cracks were created.

Results and Discussion

Two critical temperature differences were found through the quenching tests. One of them was the 74°C temperature difference above which a crack initiation began. The other was the 600°C temperature difference at which crack propagations occurred markedly and the specimens were broken down. Within the temperature difference range of 25°C to 600°C, the increased surface area caused by surface cracks was shown in Fig. 1 and the relation was expressed as a linear equation, that is

$$\begin{cases} S_V = 0.1545\ (\Delta T - 74) & T \geq 74 \\ S_V = 0 & T < 74 \end{cases}$$

where $S_V(cm^{-1})$ is the surface area of the cracks per unit volume and $\Delta T(°C)$

is the temperature difference.

The fractional release of Na and Cs from the quenched specimen, however, did not increase linearly, and was almost constant in the region of the temperature difference up to 500°C. This fact indicates that the leaching from surface cracks is strongly dependent on the crack aperture on the surface of specimens.[1)]

Concerning the lower critical temperature difference of 74°C, the next relationship may be applicable to the estimation of the threshold temperature difference for crack initiation,[2)]

$$\Delta T_{th} = \frac{S(1 - \mu)}{E \cdot \alpha} \qquad \cdots\cdots\cdots \quad (1)$$

where ΔT_{th} is the threshold temperature difference, S is the tensile strength, μ is Poisson's ratio, E is Young's modulus, and α is the thermal expansion coefficient. The measured values of S, E, and α were 10.8 kg/mm^2, 7.56×10^3 kg/mm^2, and 7.8×10^{-6}/°C respectively, and μ is assumed to be 0.25. Putting these values into the equation (1), we obtain the threshold temperature difference of 137°C by the calculation. From the experimental data (Fig. 1), however, the threshold temperature difference above which the crack initiation began was 74°C, which was less than the calculated value. It should be mentioned that the value of the strength, S, was measured by means of the three point bending method and, in general, the empirical value of tensile strength is 0.5 to 0.7 times smaller than that of the bending strength. If the tensile strength is assumed to be half the measured bending strength, the calculated threshold temperature difference is 69°C, which is close to the observed value of 74°C. So, if we use the empirical tensile strength data, equation (1) may be a good approximation to estimate the threshold temperature difference which is allowed to keep the glass without cracking.

In order to explain the higher critical temperature difference of 600°C, the thermal expansion coefficient was measured in the temperature region of 50°C to 570°C. The result shows that the thermal expansion coefficient changes as follows;

50°C - 300°C	7.8×10^{-6}/°C
300°C - 500°C	9.3×10^{-6}/°C
500°C - 570°C	40.6×10^{-6}/°C

It is clear that the thermal expansion coefficient is raised one order

of magnitude from 50°C to 570°C. So when the temperature difference is 600°C, the specimen suffers drastic volume change immediately after dropping into water at room temperature. We think this is one of the reasons why the specimen is broken down under the extreme thermal shock condition, that is from 620°C to room temperature.

References

1) J.M. Perez, Jr., and J.H. Westsik, Jr., "Effects of Cracks on Glass Leaching" Nuclear and Chemical Waste Management, vol.2 p.165-168 (1981)

2) W.D. Kingery et al., "Introduction to Ceramics" p.816 John Wiley & Sons (1976)

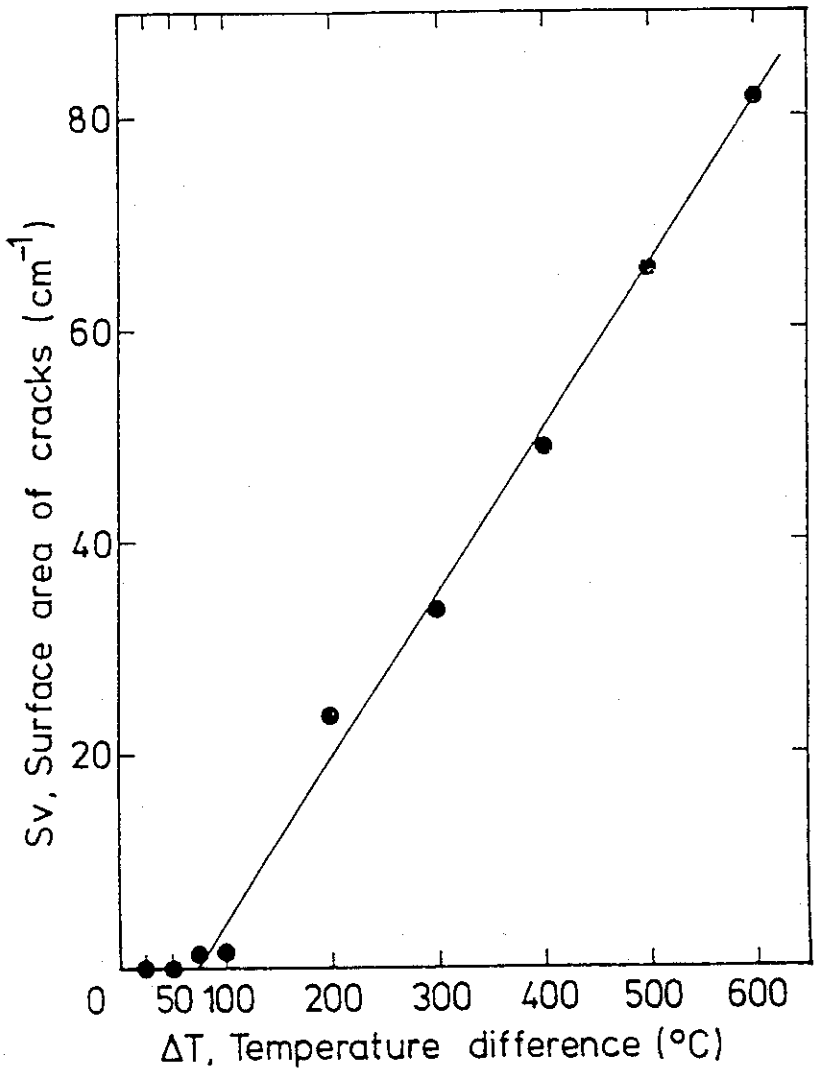

Fig. 1 Surface area of cracks vs. temperature difference

2. Development of alternative HLW form

T. Murakami

2.1 Effect of unknown phases in SYNROC

SYNROC is planned to consist of three mineral phases; hollandite, $BaAl_2Ti_6O_{16}$; perovskite, $CaTiO_3$; zirconolite, $CaZrTi_2O_7$, and also contain metal phases.[1] Additional phases, however, can occur on ordinary synthesizing conditions of SYNROC, that is, atomospheric sintering, hot-pressing and hot isostatic pressing and these phases may have an influence on physical and chemical characteristics of SYNROC.

A composition of the SYNROC specimen (A) is given in Table 1. The specimen was synthesized as follows: 1. Nonradioactive simulated HLW, which was previously calcined, was mixed with additives. 2. The mixture was calcined at 1000°C for 10 hours and subjected to hot-pressing in an N_2 atomosphere (1200°C and 600 kgf/cm^2 for 2 hours). 3. The pelletized specimen was refired at 1300°C for 25 hours. The weight loss during hot-pressing and refiring was 1.4%.

The specimen was milled to be used for X-ray diffractometry and analytical electron microscopy. The former was used for identification of mineral phases of the specimen and the latter, for elemental analysis of the minerals. The results by analytical electron microscopy have been already reported in the previous paper.[2]

Figure 1 shows an X-ray diffractogram which indicates a few low peaks occur other than peaks of hollandite, perovskite and zirconolite. Similar unidentified peaks were found in around 30 SYNROC samples which were preliminarily synthesized. Note that any phases, contained less than a few wt%, and amorphous phases cannot be detected by X-ray diffraction method.

The results of analytical electron microscopy[2] revealed that compositions of particles of minerals varied from one to another even in the same mineral phase. Accordingly, it was not certain whether all of the HLW elements were immobilized in the constituent phases as expected or not.

These results indicate that some of the HLW elements are possible to enter unidentified and undetected phases which have an influence on leaching behavior.

The difference of leaching data presented by several researchers[3,4,5] may be due to the different fomation of such unidentified and/or undetected

phases. Similar results were obtained by transmission electron microscopy.[6]

2.2 Effect of preparation conditions on distribution of radioactive waste elements among SYNROC minerals

Distribution of radioactive waste elements among SYNROC minerals is affected by preparation conditions such as redox, compositions, forming temperatures and so on.[1,7] The effect of different synthesizing conditions; conditions; atomospheric sintering, hot-pressing and hot isostatic pressing, on distribution is examined.

A composition of the SYNROC specimen (B) is given in Table 2. The composition of the additives was changed in accordance with the previous distribution data.[2] The composition of the waste oxides was also changed for the convenience of elemental analysis by energy dispersive spectroscopy. This specimen was synthesized as follows: 1. Nonradioactive simulated HLW and additives were mixed and then calcined at 1000°C for 40 hours in an N_2 atomosphere. 2. Metal powder of Ti was mixed with the above mixture because of desired redox conditions on which Mo^{6+} would be unstable. 3. They will be subjected to one of the above three synthesizing methods. At the present stage, one specimen by hot isostatic pressing (1200°C and 800 kgf/cm^2 for one hour) was obtained and nothing by the other methods.

Elemental analyses of the constituent minerals of the specimen were carried out by analytical electron microscopy (Table 3). The conspicuous features of the specimen (B) is that it had a metal phase of Mo. On the other hand, the specimen (A) did not have any metal phase and Mo entered perovskite. Such difference must bring different leach rate of Mo between the specimens (A) and (B).

Further investigations of distribution and leaching behavior are now carried out.

References

1) A.E. Ringwood et al. : Nucl. Chem. Waste Manag. 2, 287 (1981)
2) S. Tashiro (Ed.) : JAERI-M 82-145 (1982)
3) Coles, D.G. & Bazan, F. (1982) Nucl. Tech., 56, 226-237.
4) Kennedy, C. R., Flynn, K. R., Arons, R. M. & Dusek, J. T. (1982) Nucl. Tech., 56, 278-288.
5) Oversby, V. M. & Ringwood, A. E. (1982) Radioac. Waste Manag., 2, 223-237.
6) Clarke, D.R., Jantzen, C. M. & Harker, A. B. (1982) Nucl. Chem. Waste Manag., 3, 59-66.
7) Ryerson, F. J., Hoenig, C. L. & Smith, G. S. (1981) UCRL-86880.

Table 1 Composition of a SYNROC specimen (A)

Additives	wt%	Waste oxides	wt%	Waste oxides	wt%
TiO_2	54.9	MoO_3	0.93	Na_2O	1.71
Al_2O_3	6.5	MnO_2	0.14	P_2O_5	0.17
ZrO_2	10.9	Fe_2O_3	1.75	La_2O_3	0.25
CaO	10.9	CrO	0.21	Ce_2O_3	0.83
BaO	6.9	NiO	0.36	Pr_2O_3	0.13
		CoO	0.06	Nd_2O_3	0.53
Waste oxides		Ag_2O	0.02	Sm_2O_3	0.24
		CdO	0.02	Gd_2O_3	0.23
Rb_2O	0.07	TeO_2	0.12	Dy_2O_3	0.13
SrO	0.09	Cs_2O	0.53	Y_2O_3	0.20
ZrO_2	0.08	BaO	0.34		

Table 2 Composition of a SYNROC Specimen (B)

Additives	wt%	Waste oxides	wt%
TiO_2	55.4	MoO_3	0.92
CaO	13.5	MnO_2	0.14
ZrO_2	10.0	TeO_2	0.12
Al_2O_3	4.0	Cs_2O	0.52
BaO	6.3	Pr_6O_{11}	1.31
Ti(metal)	2.0	Nd_2O_3	1.20
		Na_2O	1.69
Waste oxides		Fe_2O_3	1.42
RuO_2	0.59	Cr_2O_3	0.21
PdO	0.33	NiO	0.18
SrO	0.18		

Table 3 Distribution of elements (tentative)

	Ti	Al	Ca	Zr	Ba	Sr	Mo	Fe	Cs	Pr	Nd	Na	Si
Hollandite	M	M	T	T	M	-	-	+	+	-	-	-	-
Perovskite	M	-	M	T	-	+	-	+	-	+	+	+	+
Zirconolite	M	T	M	M	-	+	-	+	-	+	+	-	+
Metal phase							+						

M: major, T: trace, +: present, -: not detected

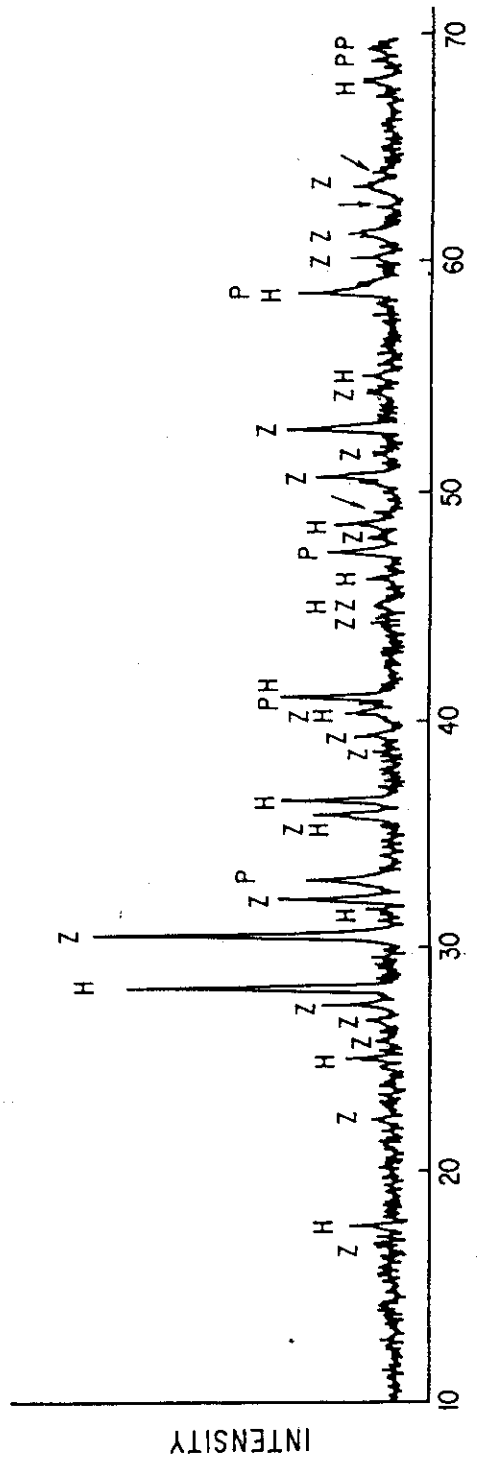

Fig. 1 An X-ray diffractogram of a SYNROC specimen (graphite monochromatized Cu Kα, 32.5 KV, 15 mA). H: hollandite, P: perovskite, Z: zirconolite. Arrows show unidentified low peaks.

3. Durability test with γ-ray irradiation of structural material for HLW storage facility

3.1 Corrosion resistance of alloys

T. Furuya

Introduction

The candidate materials for high-level waste canister and overpack are austenitic stainless steels, nickel base alloys and so on. These alloys will be exposed with high-level gamma-rays when HLW will be packed into them. It was shown that Type 304 stainless steel and Type 304L stainless steel, which belonged to austenitic stainless steel, were more suscetible to stress corrosion cracking (SCC) in boiling deionized water with gamma-rays irradiation than without irradiation in the former report [1].

In this report, in order to make these phenomena clear, gamma-rays effects on SCC of Type 304 stainless steel were studied with the electrical method.

This study was carried out in cooperation by JAERI and Kobe Steel Ltd.

Experimental

The worked electrode specimen made from Type 304 stainless steel was immersed in boiling deionized water (relative electric resistance ; $>5 \times 10^6 \Omega$ cm). The natural potential of worked electrode were measured either with gamma-rays irradiation or without irradiation. The dose rate of gamma-rays was 1.1×10^5 R/hr with Co-60. The apparatus are schematically shown in Fig. 1.

Results and discussion

The changes of natural potentials with and without gamma-rays irradiation were shown in Fig. 2.

The natural potential of Type 304 stainless steel changed immeadiately to noble potential when the worked electrode was irradiated with gamma-rays, and the potential stayed at about -150 mV vs. SEC after 60 hrs, and then gamma-rays irradiation was stopped, the potential changed immeadiately to less noble direction but did not recover to the original potential. On the other hand, the natural potential without any irradiation changed slowly to noble potential, and the potential stayed at about -330 mV vs. SEC after 45 hrs. These phenomena suggested that oxidants such as oxygen generated by reason of hydrolysis of water with gamma-rays irradiation.

In order to make these oxidated conditions without any irradiation, each potential of -600, -400, -350, -300 and -250 mV vs. SEC was applied to double U-bend specimens with potentiostat. The results were shown in Fig. 3. Although inner specimens of double U-bend at -600, -400 and -350 mV vs. SEC were not cracked, the others were cracked after immersion for 7 days.

From these results it was concluded that gamma-rays irradiation caused double U-bend specimen of sensitized Type 304 stainless steel to change to SCC generation potential.

Reference

[1] T. Furuya, S. Muraoka, S. Tashiro, K. Araki H. Tomari, K. Fujiwara and T. Fukuzuka; JAERI-M 82-061 (1982).

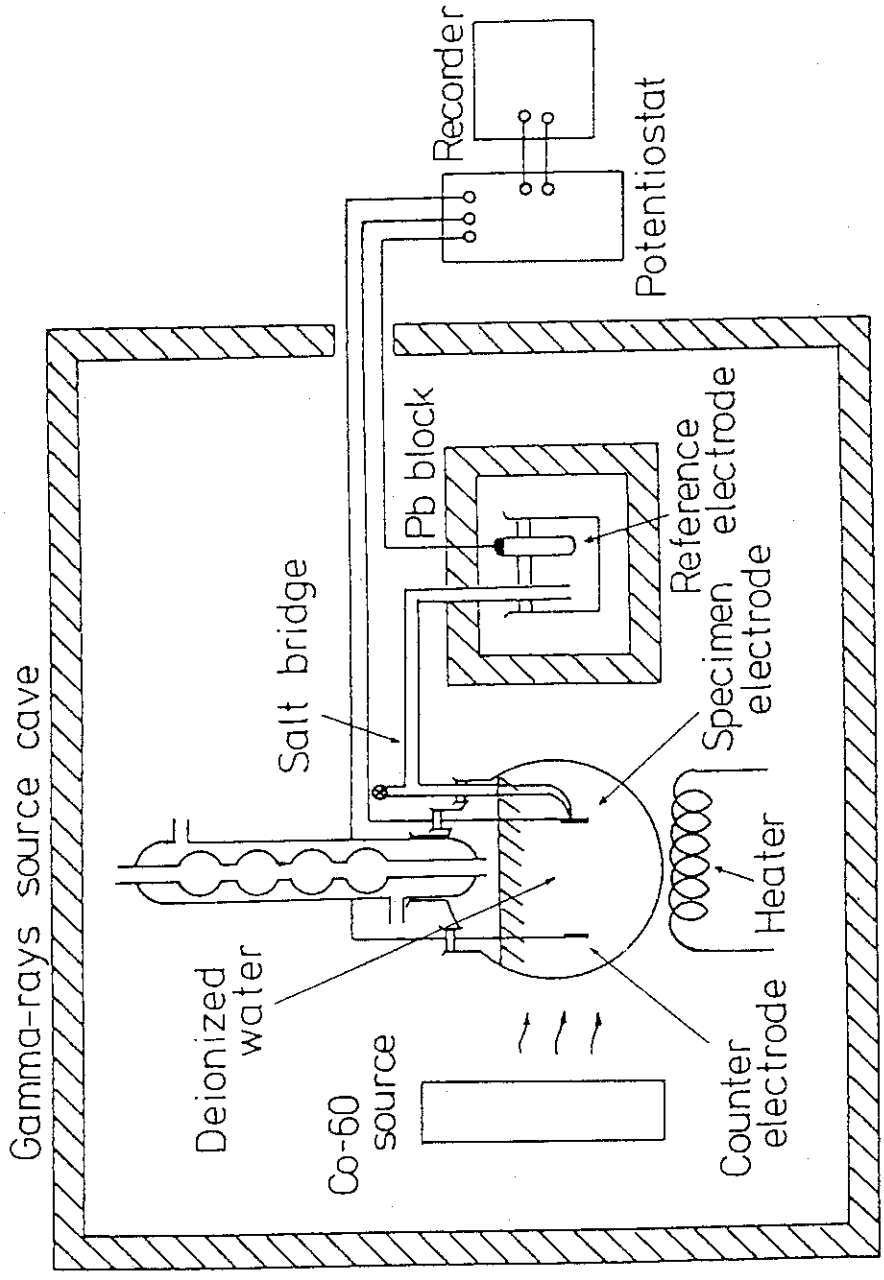

Fig. 1. Schematic diagram of electrochemical measurement with gamma-rays irradiation

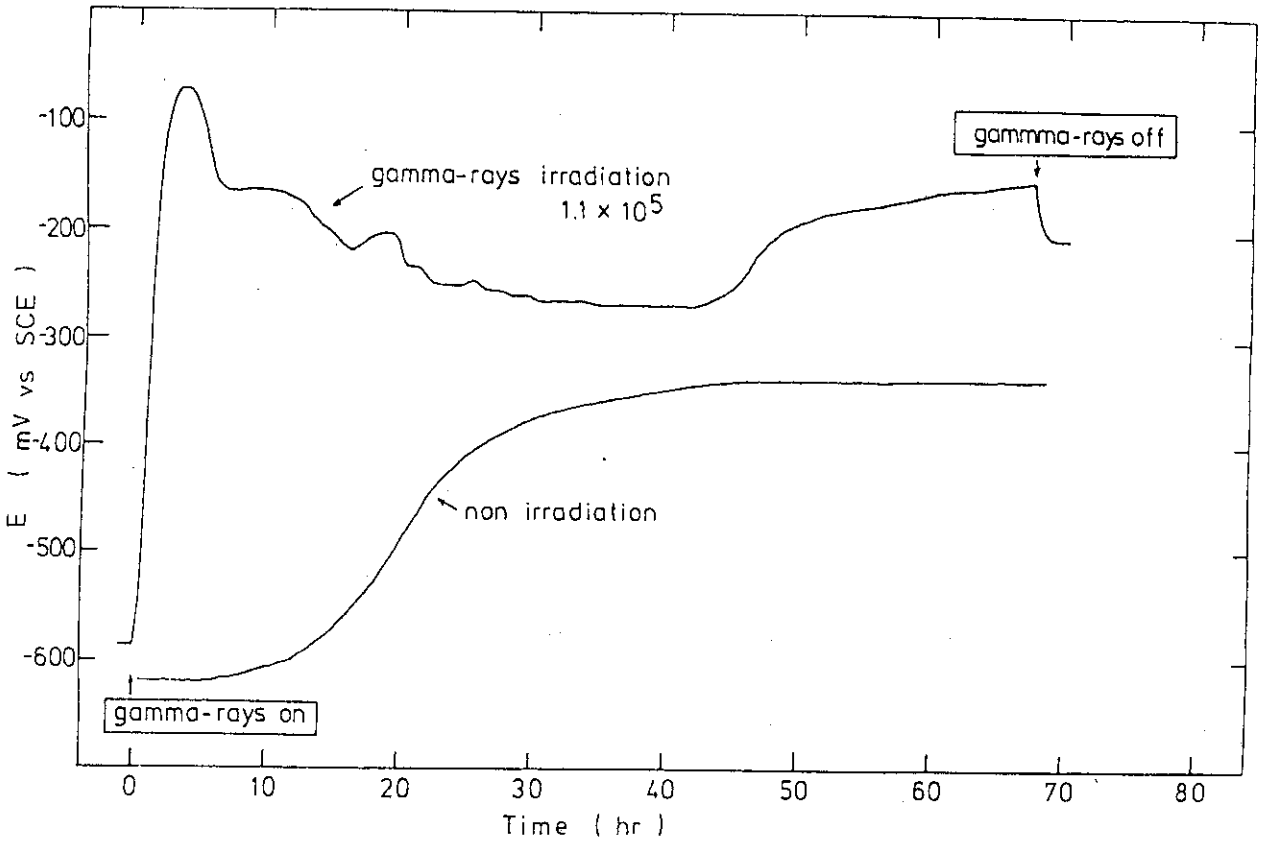

Fig. 2 Effects of gamma rays irradiation on natural potential of sensitized Type 304 stainless steel immersed in boiling deionized water

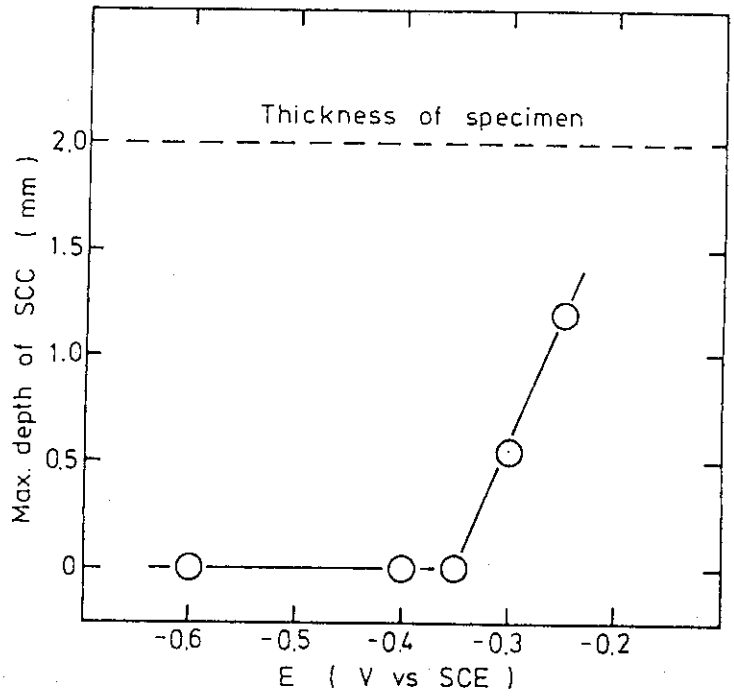

Fig. 3 Effect of applied potential on SCC of sensitized Type 304 stainless steel immersed in boiling deionized water for 7 days.

4. Safety evaluation of geologic disposal

4.1 Nuclide migration code

H. Kimura

On the safety assessment of radionuclide migration from the high level waste repository, the improvement of nuclide migration code was carried out. By the nuclide migration code developed in FY1981 using direct-simulation method[1] (Monte-Carlo method), the calculated results have large fluctuation in the case of a few number of particle distribution. We have introduced smoothing method to obtain the exact particle distribution and radioactive inventory. Benchmark test was performed by using INTRACOIN International Nuclide Transport Code Intercomparison)[2] data, and reasonable results were obtained. Furthermore, discharge rates to ground surface of radioactive nuclides from the reference high level waste repository were calculated.

Smoothing method

Because leaching of nuclide from the waste form is continuous, superimpose procedure is needed in the Monte-Carlo method. Leaching of nuclide is divided into some instantaneous release, and each instantaneous release is given by staggering the release time of one instantaneous release. After superimpose procedure was carried out, new particles are regenerated according to the Gaussian distribution on the basis of the obtained particle distribution, and activities are determined by solving the Bateman's equations.

Numerical results

Input data of benchmark test is shown in Table 1, and calculated results are shown in Table 2 and Table 3, respectively case-1 and case-2. Case-1 is the $^{245}Cm \rightarrow {}^{237}Np \rightarrow {}^{233}U$ decay chain, and case-2 is the $^{234}U \rightarrow {}^{230}Th \rightarrow {}^{226}Ra$ decay chain. The migration profiles of our model in case-1 and case-2 have enough agreement with other models.

The reference high level waste repository is assumed in the calculation as follows.

(1) The pass length to environment from the repository is 5 km.
(2) The geologic media is composed by three-layer, and each layer pass length is respectively 3.6 km, 1.0 km and 0.4 km.
(3) Leaching from the waste form starts 1000 years after reprocessing,

and leaching period is 3×10^5 years.

Nuclide inventory is shown in Table 4, and it is calculated by ORIGEN code[3]. The other input data is shown in Table 5, and the calculated result is shown in Fig. 1. The calculation shows that main effect to human dose over a long period of time is due to ^{237}Np decay chain as the results of many researchers.

Table 1 INTRACOIN study input data

nuclide	half-life (yr)	inventory (Ci)	retardation factor	dispersion coefficient (m^2/yr)	leach-time (yr)	migration length (m)	flow-rate (m^3/yr)
^{245}Cm	8.50×10^3	0.7	60	50.0	100000	500.0	100.0
^{237}Np (case-1)	2.14×10^6	1.0	200	50.0	100000	500.0	100.0
^{233}U	1.59×10^5	0.004	60	50.0	100000	500.0	100.0
^{234}U	2.45×10^5	1.0	300	50.0	100000	500.0	100.0
^{230}Th (case-2)	7.70×10^4	0.01	20000	50.0	100000	500.0	100.0
^{226}Ra	1.60×10^3	0.004	10000	50.0	100000	500.0	100.0

* ground water velocity ; 1.0 (m/yr)

** porosity ; 0.01

Table 2 INTRACOIN study calculation results (case-1)

nuclide \ CODE		SWENT	MMT1D	UCB-NE	RANCH	Our-model
^{245}Cm	$T_{0.5}$ *	1.64×10^{4}	1.55×10^{4}	1.78×10^{4}	1.58×10^{4}	1.40×10^{4}
	T_{max} **	2.64×10^{4}	2.50×10^{4}	2.86×10^{4}	2.55×10^{4}	2.45×10^{4}
	C_{max} ***	3.73×10^{-7}	4.23×10^{-7}	2.53×10^{-7}	3.84×10^{-7}	4.26×10^{-7}
^{237}Np	$T_{0.5}$	8.32×10^{4}	7.48×10^{4}	9.38×10^{4}	8.14×10^{4}	7.80×10^{4}
	T_{max}	1.42×10^{5}	1.32×10^{5}	1.54×10^{5}	1.40×10^{5}	1.40×10^{5}
	C_{max}	7.92×10^{-6}	7.45×10^{-6}	6.97×10^{-6}	7.79×10^{-6}	6.85×10^{-6}
^{233}U	$T_{0.5}$	6.21×10^{4}	5.76×10^{4}	6.76×10^{4}	6.18×10^{4}	6.70×10^{4}
	T_{max}	1.12×10^{5}	1.06×10^{5}	1.16×10^{5}	1.12×10^{5}	1.20×10^{5}
	C_{max}	5.83×10^{-6}	5.51×10^{-6}	5.73×10^{-6}	5.75×10^{-6}	5.77×10^{-6}

* $T_{0.5}$ is the time when the concentration reachs half of maximum value

** T_{max} is the time when the concentration reachs maximum value

*** C_{max} means the maximum value of concentration (μCi/ml)

Table 3 INTRACOIN study calculation results (case-2)

nuclide \ CODE		SWENT	MMTID	UCB-NE	RANCH	Our-model
^{234}U	$T_{0.5}$	1.07×10^{5}	9.90×10^{4}	1.04×10^{5}	1.04×10^{5}	9.90×10^{4}
	T_{max}	1.67×10^{5}	1.62×10^{5}	1.65×10^{5}	1.65×10^{5}	1.65×10^{5}
	C_{max}	3.98×10^{-6}	4.24×10^{-6}	3.94×10^{-6}	3.94×10^{-6}	3.88×10^{-6}
^{230}Th	$T_{0.5}$	1.47×10^{5}	1.36×10^{5}	1.45×10^{5}	1.45×10^{5}	1.40×10^{5}
	T_{max}	2.30×10^{5}	2.13×10^{5}	2.29×10^{5}	2.28×10^{5}	2.30×10^{5}
	C_{max}	3.50×10^{-8}	4.26×10^{-8}	3.47×10^{-8}	3.47×10^{-8}	3.69×10^{-8}
^{226}Ra	$T_{0.5}$	1.50×10^{5}	1.39×10^{5}	1.47×10^{5}	1.45×10^{5}	1.42×10^{5}
	T_{max}	2.32×10^{5}	2.31×10^{5}	2.30×10^{5}	2.28×10^{5}	2.30×10^{5}
	C_{max}	7.08×10^{-8}	5.30×10^{-8}	6.93×10^{-8}	6.94×10^{-8}	7.39×10^{-8}

Table 4 HLW inventory at 1000 years after reprocessing (per $1GW_eYr$ generation)

nuclide	decay const. (1/yr)	activity (Ci)	atom number
^{245}Cm	8.15×10^{-5}	9.42	1.31×10^{23}
^{237}Np	3.24×10^{-7}	16.5	5.97×10^{25}
^{233}U	4.36×10^{-6}	6.21×10^{-2}	1.69×10^{22}
^{229}Th	9.49×10^{-5}	2.76×10^{-3}	3.39×10^{19}
^{242}Pu	1.84×10^{-6}	2.57×10^{-1}	1.64×10^{23}
^{238}U	1.55×10^{-10}	5.73×10^{-2}	4.35×10^{26}
^{234}U	2.83×10^{-6}	3.62×10^{-1}	1.51×10^{23}
^{230}Th	8.66×10^{-6}	2.73×10^{-3}	3.67×10^{20}
^{226}Ra	4.33×10^{-4}	4.67×10^{-4}	1.26×10^{18}
^{243}Am	9.40×10^{-5}	5.37×10^{2}	6.90×10^{24}
^{239}Pu	2.88×10^{-5}	73.0	2.99×10^{24}
^{235}U	9.85×10^{-10}	3.53×10^{-3}	4.22×10^{24}
^{231}Pa	2.11×10^{-5}	1.81×10^{-4}	9.91×10^{18}
^{240}Pu	1.07×10^{-4}	2.40×10^{2}	2.73×10^{24}
^{236}U	2.96×10^{-8}	6.21×10^{-2}	2.51×10^{24}
^{232}Th	4.91×10^{-11}	5.48×10^{-9}	1.30×10^{20}

Table 5 Input data for three-layer calculation

layer	retardation factor							water velocity (m/yr)	porosity
	Cm	Am	Pu	Np	U,Pa	Th	Ra		
I (3.6km)	100000	3000000	40000	10000	1000	400000	40000	100.0	0.01
II (1.0km)	50000	1500000	20000	5000	500	200000	20000	50.0	0.02
III (0.4km)	10000	300000	4000	1000	100	40000	4000	20.0	0.05

Leach time ; 3×10^5 (yr)

Flow rate ; 100 (m^3/yr)

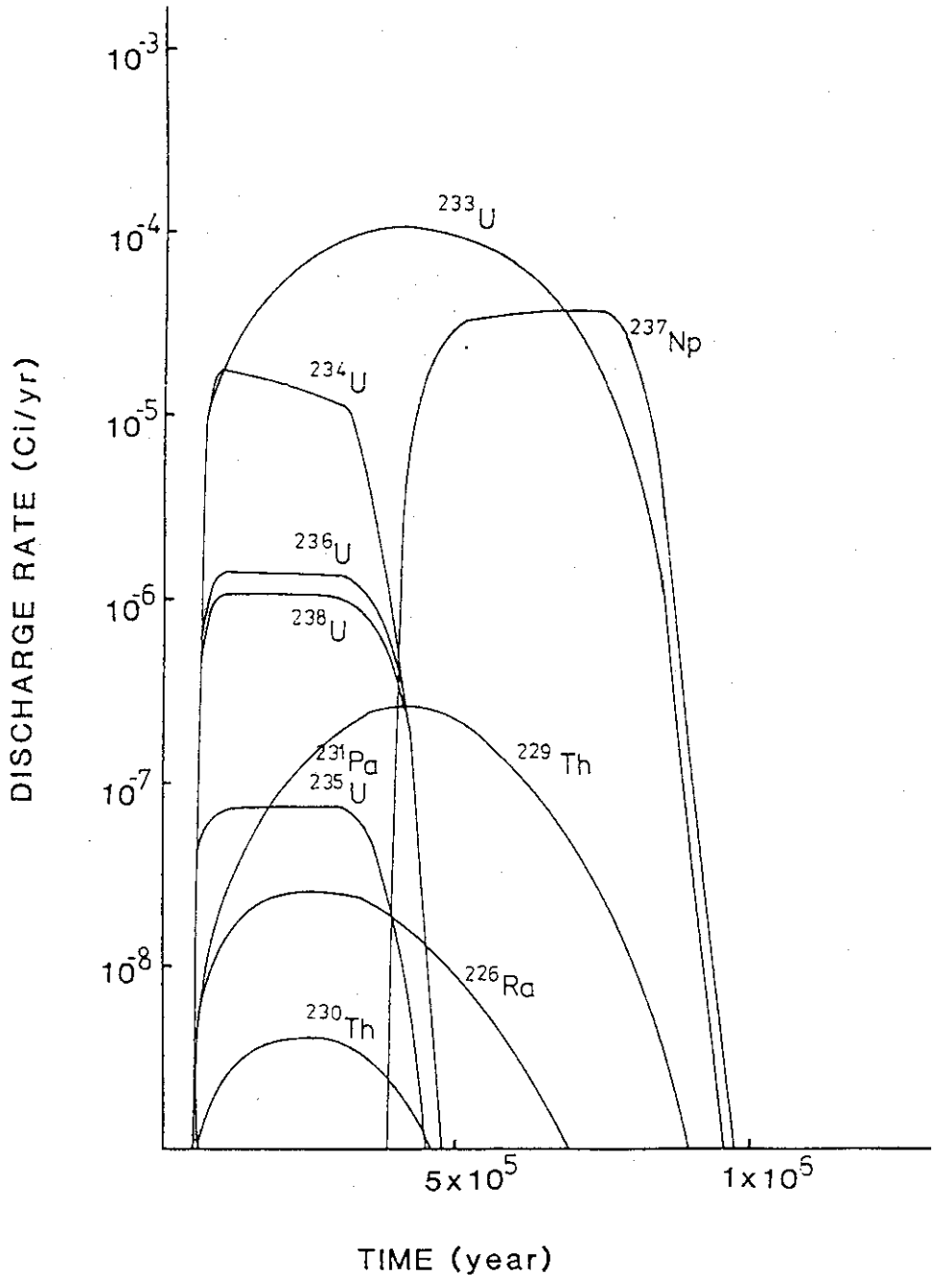

Fig.1 Discharge rates to ground surface of HLW

4.2 Field tests

4.2.1 Buffer mass test in SITU

S. Muraoka

Buffer (or Backfill) material is expected to bear important role as an engineered barrier in a multi-barrier system of geological disposal of high-level waste. Many R & D studies have been carried out in the USA and Sweden as a program of Basalt Project and KBS Project respectively.

In Japan, on the other hand, the study has been started few years ago. The candidate materials for backfilling deposition holes, seal tunnels and shaft should possess the following properties

1. Enough Plasticity
2. High Swelling Capacity
3. High Ion Exchange Capacity
4. Low Permeability
5. Good Thermal Conductivity

Bentonite (Smectite) is a promissing material mostly abundant in Japan.

Prior to the field test, KUNIGEL VA bentonite was screened out by the X-ray diffraction method. This material is Na type bentonite and its chemical composition and some physical properties are shown in Table 1. This clay was solidified and characterized about the relationship between, thermal conductivity and specific heat, and uniaxial compressive strength. The results were shown in Fig. 1.

In SITU test has been carried out in the mine of 380 m depth from the surface of Akenobe Mine located in Hyogo Prefecture, Japan. The type of rock was schalstein of Perian age. The experimental vertical hole was drilled to 330 mm radius and 3.3 m depth. After drilling, several fissures were observed on the inner wall of the hole as shown in Fig. 2 and the water seepage was found at three parts of these fissures. The quantity of the ground water seeped naturally were 2.6 liter for first 10 days just after drilling. In this hole KUNIGEL VA was solidified by use of 20 ton oil pressurized jack with a pressure of 20 Kg/cm^2. An electric heater and thermocouples were emplaced such a geometry as shown in Fig. 3. After heating test, thermal conductivity was calculated from temperature distribution in the bentonite and the change of water content due to heating were measured. These results were shown in Fig. 4 and Fig. 5.

Table 1 Chemical composition and physical properties of KUNIGEL VA

Chemical composition (%)		Physical property	
SiO_2	65 ∿ 75	specific gravity	2.4
Al_2O_3	14 ∿ 17	grain size (mesh)	300
Fe_2O_3	1.9 ∿ 2.4	apparent specific gravity	0.50-0.65
CaO	1.2 ∿ 1.9	pH	9.2-10.5
MgO	1.8 ∿ 3.0	water content (%)	<8
Na_2O	1.8 ∿ 2.5	swelling capacity (cc/g)	>20
K_2O	0.5 ∿ 1.0		
Ig-loss	4.5 ∿ 5.0		

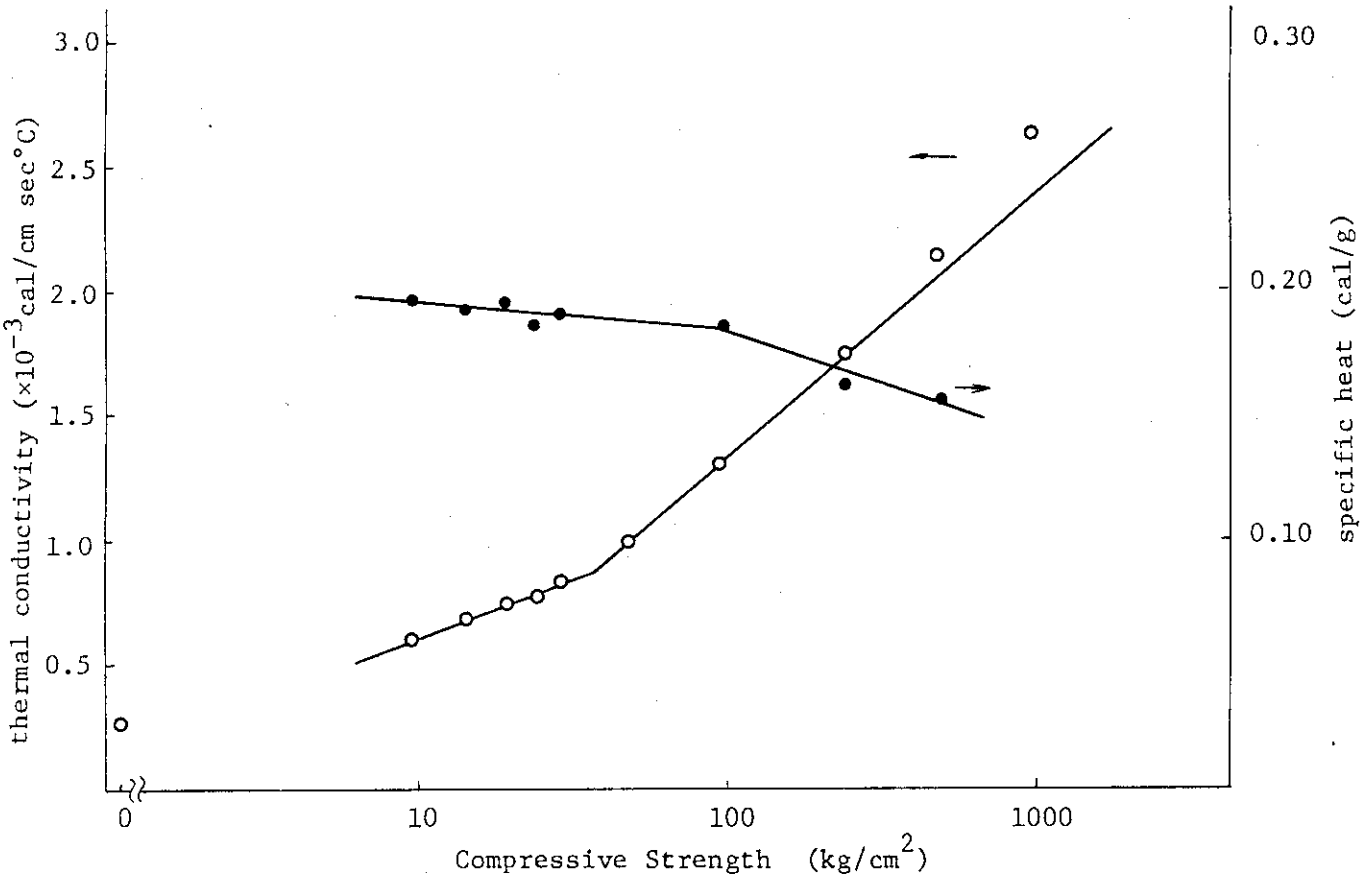

Fig. 1 Relation between compressive strength and thermal conductivity, specific heat

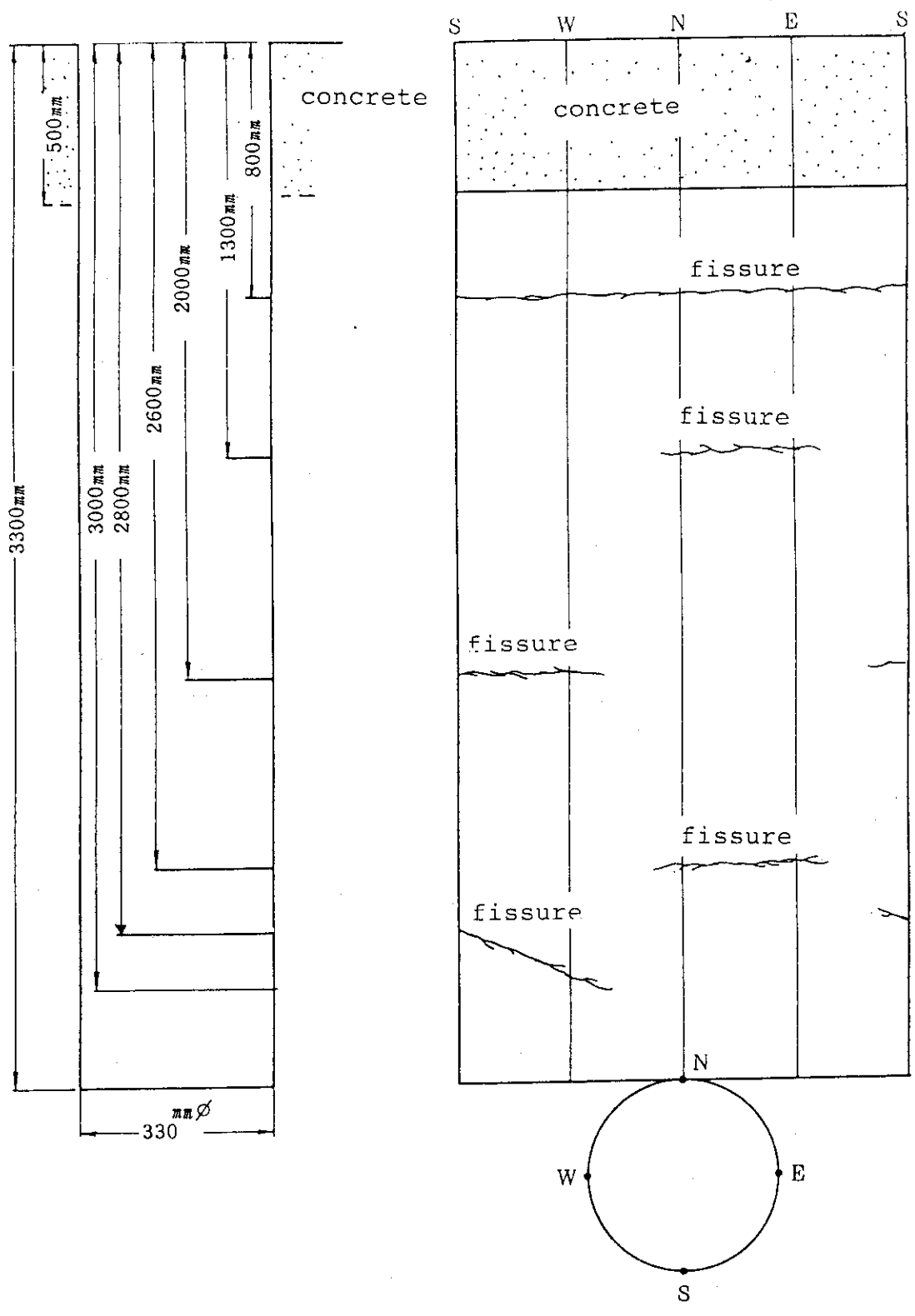

Fig.2 Inner surface of test hole

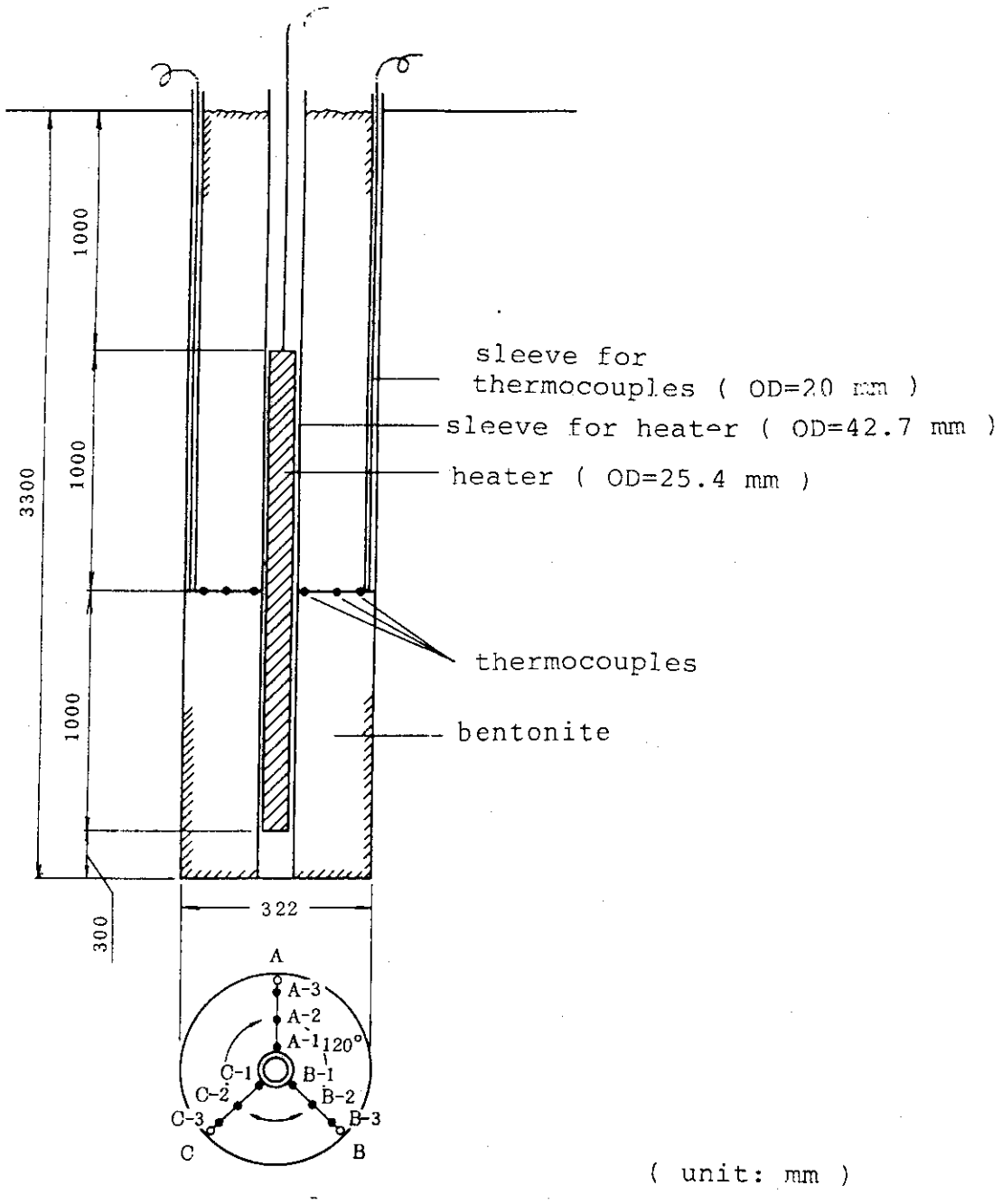

Fig. 3 Arrangement of heater and thermocouple

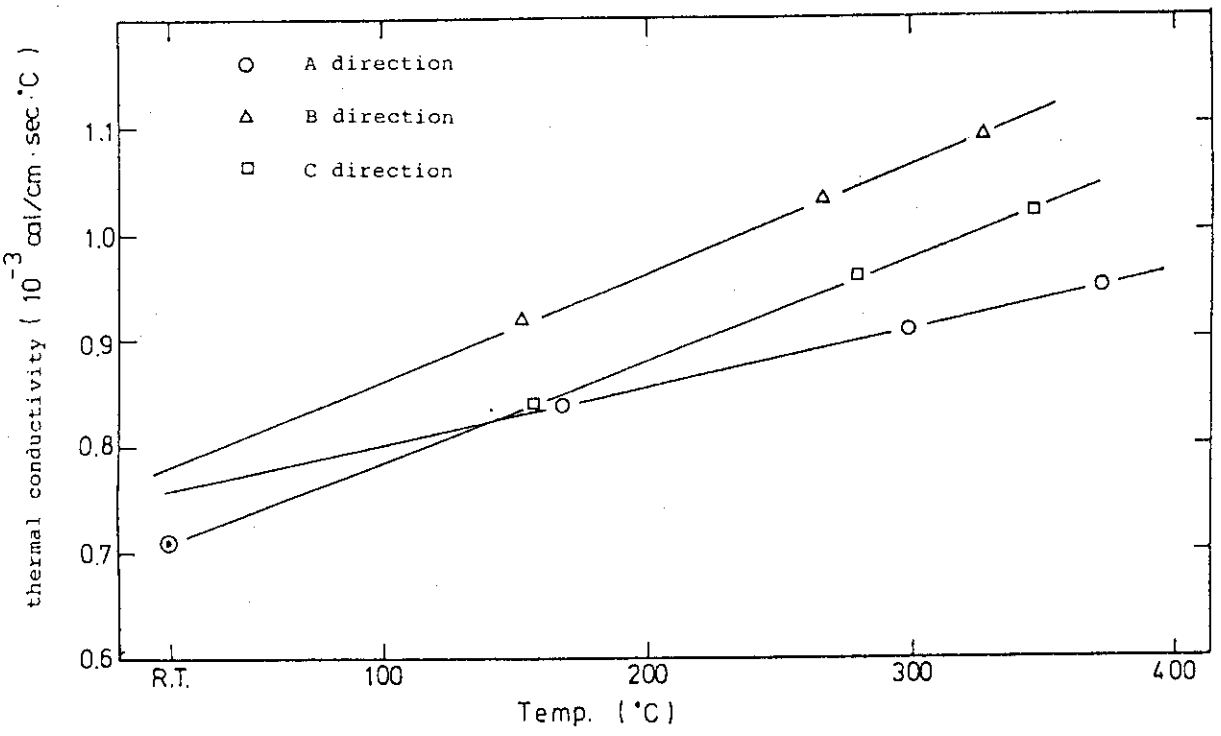

Fig. 4 Temperature dependency on thermal conductivity

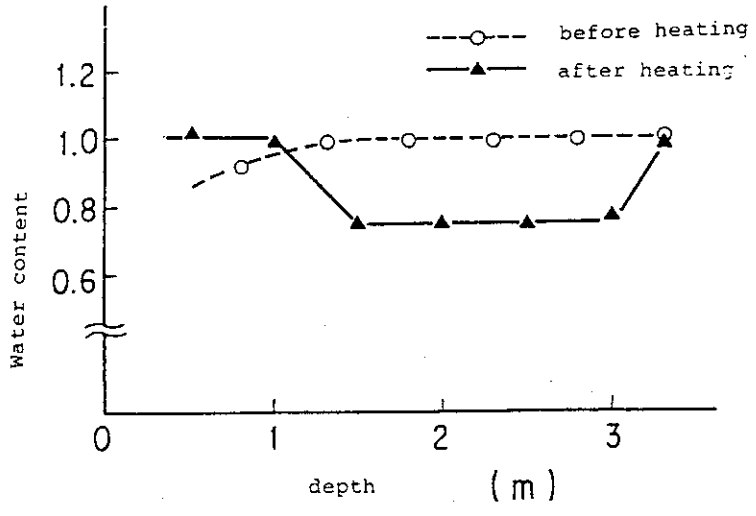

Fig. 5 Change of water content in bentonite

4.2.2 Measurements of permeability of a rock mass and the thermomechanical effect on permeability

K. Shimooka

One of the most important driving forces for HLW migration is the ground water flow.

The movement of the ground water is mainly through fractures especially in crystalline rock masses.

Moreover, the thermomechanical effect from the decay heat on fractures should be considered.

Therefore the experiments to investigate the relation between permeability-fracture-heat were conducted.

Experiment

1) Measurement of the permeability

The Packer Method was adopted to measure the permeability of a rock mass, under three temperature conditions, i.e. at normal, at elevated and at normal after heating.

The distance between two rubber packers was set to 45 cm and warer was supplied with a pressure of 3, 6, 10 and 18 kg/cm^2.

Permeability was calculated with using supplied water pressure and the water volume according to the formula;

$$K = \frac{Q}{2\pi LH} \sin^{-1}\left(\frac{L}{2r}\right)$$

$$= \frac{Q}{2\pi LH} \ln\left[\frac{L}{2r} + \sqrt{\left(\frac{L}{2r}\right)^2 + 1}\right]$$

in the case of $L/r >> 1$

$$K \fallingdotseq \frac{Q}{2\pi LH} \ln\frac{L}{r}$$

where, K is permeability (cm/sec)
Q is flow rate (cm^3/sec)
L is length of the measured section (cm)
H is injection pressure (cm H_2O)
r is radious of the borehole (cm)

2) Survey method of the fractures in a borehole

Specific resistance in the borehole was measured by the micro-resistivity method.
From its results, the points showing anormalistic change of the specific

resistance were counted as fractures.

Results and Discussion

The permeability of the rock mass at normal temperature was below detectable limits in all tried section.

However, permeability at the elevated rock-temperature was measured and calculated at an order of 10^{-6} cm/sec.

On the other hand, measurement of fractures in the borehole by the resistivity method showed that the apparent fractures were increased by heating the rock mass.

Especially, in the vicinity of the heater, high increase of the apparent fractures was observed.

In the low-temperature section where no fracture change was observed during heating, permeability also showed no change.

These results were interpreted that the permeability was largely dependent upon the rock temperature, that is the change of the fractures by thermomechanical effect.

4.3 Laboratory tests

4.3.1 Sorption behavior of cesium on granite K. Shimooka, T. Yanagida

Sorption behavior of cesium on granite has been studied.

Distribution coefficient between fresh granite and cesium solution was measured and its results of sorption dependency on concentration and contact time was shown in the previous progress report (1982).

But there remained a question that the distribution coefficient of the fresh and intact rock sample could not present a required value to evaluate a nuclide migration in the rock mass, since ground water could scarcely flow in the virtually impermeable rock.

Therefore, the distribution coefficient of the weathered rock material sampled from the ground water flow path in the granite rock mass at Inada was measured and compared with that of fresh rock.

Experiment

1) Measurement of K_d

Experimental conditions were arranged as same as those of the previous batch tests for the fresh rock, i.e.

a) the ratio of solution volume/rock weight is 100 ml/g,
b) initial concentration of C_s is 10^{-5}, 10^{-4}, 10^{-3}, 10^{-2}, 10^{-1}, 1 and 10 μg/ml,
c) partical size is under 0.25 mm,
d) experimental temperature is room temperature.

2) Characteristics of the weatherd rock

The composition of the weatherd rock was identified by X-ray diffraction method.

Results and discussion

Results indicated that the weathered granite had the similar tendency to fresh granite on the influence of cesium concentration and the contact time.

However, the distribution coefficient of the weathered granite showed one order higher value at around 2.7×10^3 ml/g than that of fresh rock as shown in Fig. 1.

On the other hand, X-ray diffraction patterns of the weathered granite indicated that montmorillonite clay minerals were included in it.

Therefore, the reason of the difference of K_d was interpreted that the weathered granite was carring the altered material such as montmorillonite clay minerals which have high ion exchange capacity compared with other minerals consisting granite.

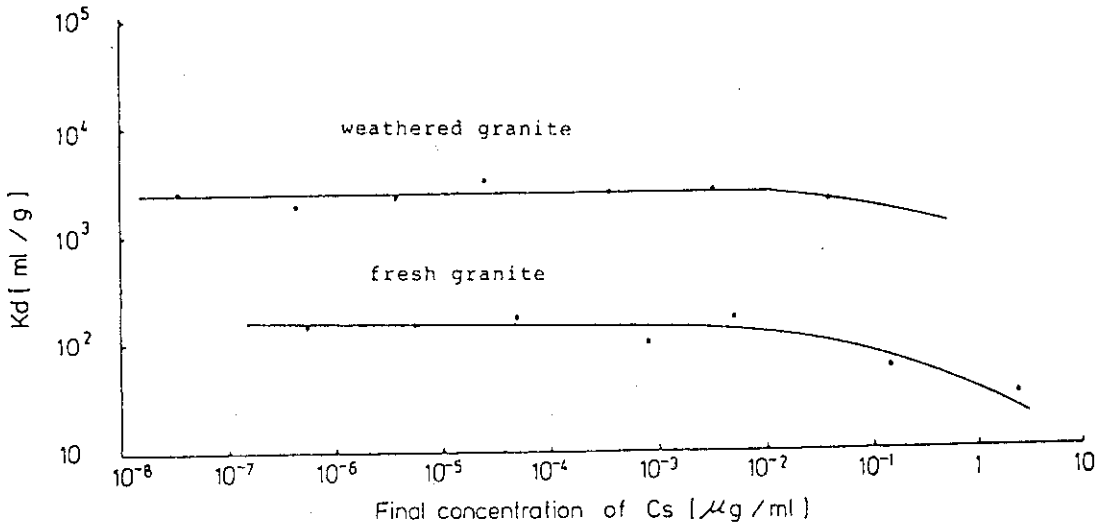

Fig. 1

4.3.2 Interaction of waste radionuclides with geologic materials under high temperature

Introduction

The main threats to the effective isolation of radionuclides from biosphare are disolution of the waste and subsequent radionuclides transport by ground water from repository in deep geological formations. Nuclide release from the repository is controlled by the hydrogeological and geochemical interactions under the repository conditions.

For the assessment of the performance of natural barrier, they are fundamental to investigate the interaction of potential waste forms with ground water under near-field conditions and adsorptive behavior of radionuclides to rocks. The experiments were designed to facilitate the study of waste-rock interaction and sorption of nuclides to rocks. High temperature such as 300°C was used to accelerate hydrothermal interactions.

(1) Hydrothermal interactions between simulated high-level waste glass and natural rocks

M. Kumata

Experimental

The experiment was carried out in a pressure-vessels, the reactants being contained in a deformable, inert, gold capsule. Starting materials were borosilicate glass, granite, basalt and deionised water. The glass contained approximately 20 wt% of simulated fission product oxides as a calcined simulated high-level liquid waste (Table 1). Solid reactants were in powdered form (-200 mesh) and small chips. Samples prepared for this experiment were shown in Table 2. The initial ratio of fluid and solis was 10 : 1, and the temperature was nominally 300°C and the pressure was 300 bar. The run duration was 30 days.

The residual solid and liquid phases from heated capsules were saved for analyses. The solid phases were dried for X-ray diffraction analysis, an optical microscopy, scanning electron microscopy (SEM) and electron probe micro analysis (EPMA). The liquid phases were diluted and were centrifuged for analyses with atomic absorption spectrophotometry (ASS) and inductively coupled plasma atomic emission spectroscopy (ICP).

Results and discussion

Eleven elements were analyzed for the solutions, diluted the liquid phases of run products from hydrothermally terated mixtures of granite or

basalt with simulated HLW glass, by means of AAS and ICP. Sodium and cesium were analyzed by AAS. Magnesium, aluminium, silicon, potasium, calcium, manganese, iron, strontium and molybdenum were analyzed by ICP.

Analysis of molybdenum for the liquid phases shows that the simulated HLW glass dissolved completely under these experimental conditions. Strontium, however, was not detected from sampled solutions at all. Data of chemical analysis for the liquid phases were listed in Table 3.

Ahalyses of the solid phases by optical microscopy, X-ray diffraction analysis and SEM showed a few new crystalline phases which were formed during hydrothermal treatment (Fig. 1). One of them was analyzed with EPMA and Fig. 2 shows secondary electron image and its characteristic X-ray images. It seems that the crystalline phase is mainly composed of silicon, aluminium, sodium and cesium.

When HLW glass coexist with natural rocks and water, a part of cesium element released from simulated HLW glass to liquid phase may be eliminated from the liquid phase due to formation of a new crystalline phase such as aluminosilicate, and almost all of cesium were still remained in the liquid under these experimental conditions.

References

1) G.J. McCarthy et al. (1978); "Simulated high-level waste-basalt interaction experiments first interim progress report" RHO-BWI-C-12.
2) S. Komarneni et al. (1980); "Hydrothermal interactions of ceasium and strontium phases from spent unreprocessed fuel with basalt phases and basalt" RHO-BWI-C-70.
3) G.J. McCarthy et al. (1979); "Hydrothermal reactivity of simulated nuclear waste forms and water-catalysed waste-rock interactions" Scientific Basis for Nuclear Waste Management, vol.1, pp.329-340.
4) S. Komarneni et al. (1981); "Hydrothermal interactions of basalts with Cs and Sr of spent fuel elements" J. inorg. nucl. Chem., vol. 43, pp. 1967-1975.
5) D. Savage and N.A. Chapman; "Hydrothermal behaviour of simulated waste glass and waste-rock interaction under repository condition" Harwell Lab. (unpublished).
6) W.P. Freeborn et al. (1980); "Shale rocks as nuclear waste repositories: Hydrothermal reactions with glass, ceramic and spent fuel waste forms"

Scientific Basis for Nuclear Waste Manegement, vol.2; pp.499-506.

7) L.V. Benson and L.S. Teague (1979); "Study of rock-water-nuclear waste interactions in the Pasco Basin, Washington" LBL-9677.

8) D. Savage (1981); "Geochemical factors controlling the nuclide release sorce-term in granite : Rock-water interactions" ENPU 81-8.

9) N.A. Chapman et al. (1981); "Mechanisms of dissolution of radioactive waste storage glasses cesium migration from a granitic repository" Proc. MRS Con. 'Scientific Basis for Nuclear Waste Management'.

10) G.J. McCarthy et al. (1978); "Interactions between nuclear waste and surrounding rock" Nature, vol. 273, pp.216-217.

11) N. Sasaki et al. (1982); "Alteration of glass and crystalline ceramic nuclear waste forms under hydrothermal conditions" Ceramic Bulletin, vol. 62, No.6, pp. 649-655.

Table 1 Composition of simulated HLW glass*

Oxide	Wt%	Oxide	Wt%
(waste oxide)		TeO_2	0.24
Rb_2O	0.14	Cs_2O	1.05
SrO	0.36	BaO	0.67
ZrO_2	1.77	Na_2O	3.42
MoO_3	1.87	P_2O_5	0.35
MnO	0.28	Cr_2O_3	0.41
Fe_2O_3	3.50	RE_2O_3	5.04
CoO	0.13	(glass forming additives)	
NiO	0.71		
Ag_2O	0.03	SiO_2	48.45
CdO	0.03	Na_2O**	10.44
		B_2O_3	21.11

* After Y.KIRIYAMA et al.(1980) ; waste loading 20 wt%, fission product loading 11.3 wt%.

** Total Na_2O = 13.86 wt%

Table 2 Sample prepared

Sample No.	Material*
3	powdered HLW glass and powdered granite
4	powdered HLW glass and powdered basalt
8	HLW glass chips
9	powdered HLW glass and granite chips
10	powdered HLW glass and basalt chips

* Added to deionised water.

Table 3 Major Element Concentration (ppm)

Sample No.	3	4	8	9	10
Si	190	200	280	170	160
Na	2800	3300	9300	3400	4300
Fe	1	2	1	-	-
Mn	-	-	1	-	-
Al	6	7	-	-	-
Mg	1	4	-	-	-
Ca	3	3	3	3	3
K	350	180	40	140	190
Cs	200	260	640	200	260
Mo	600	850	2000	700	970
Sr	-	-	-	-	-

- : not detected

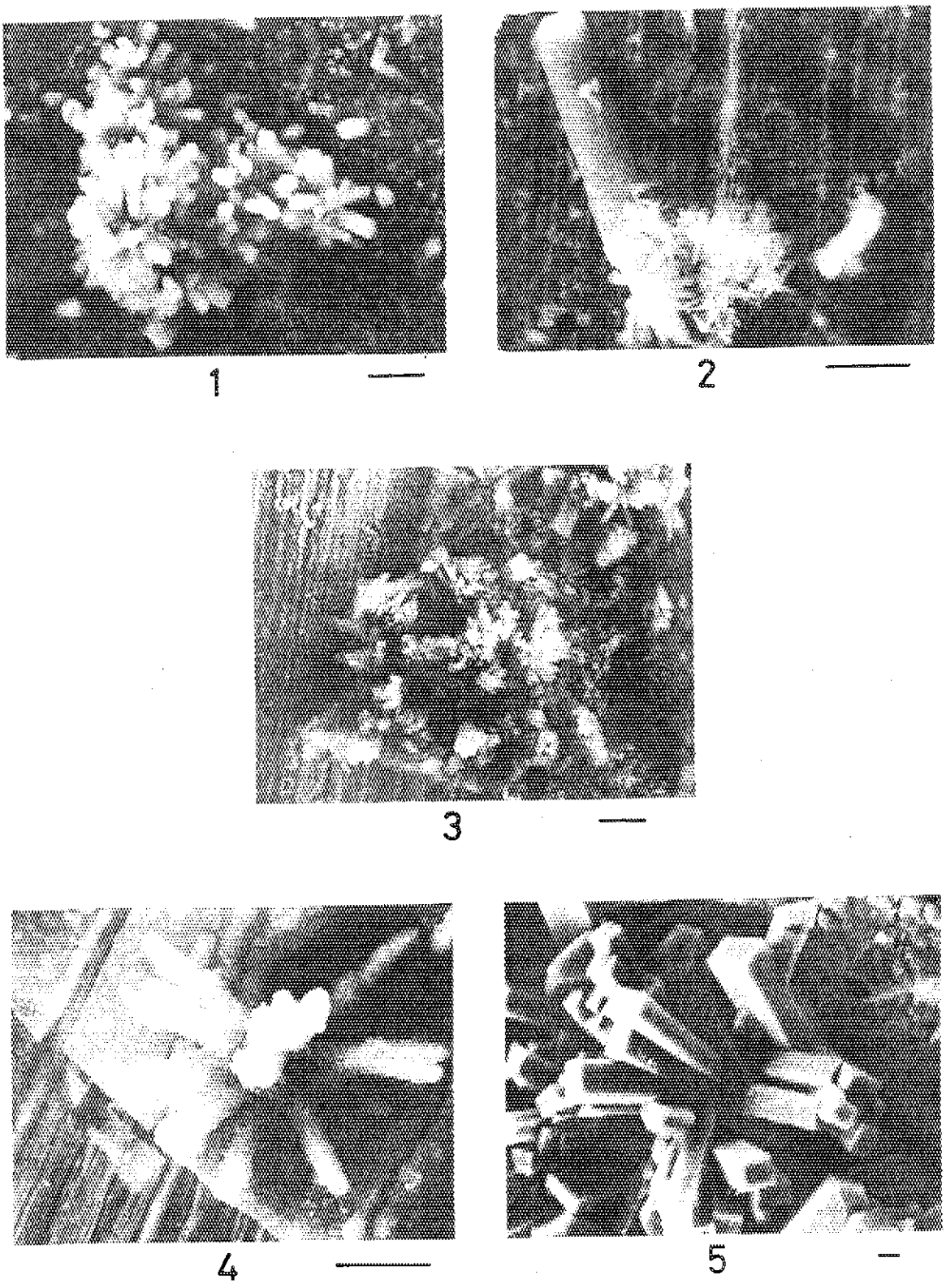

Fig. 1 Scanning electron micrographs showing new crystalline forms after hydrothermal treatment (bar = 5 μm).

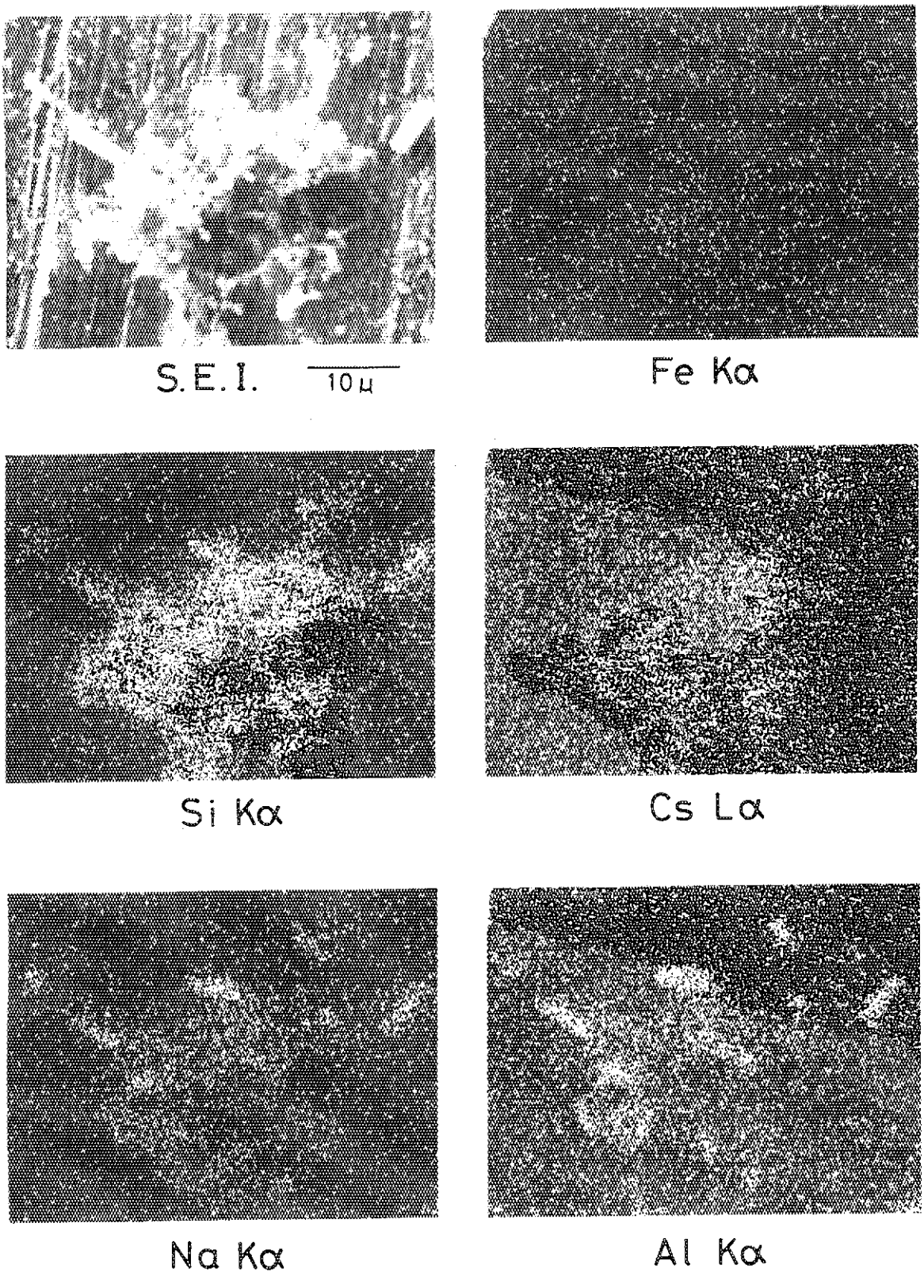

Fig. 2 The secondary electrom image and its characteristic X-ray images of hydrothermal product.

(2) Sorption behavior of Cs on rocks under high temperature

K. Amemiya

Experimental

The rocks used in the experiments were biotite granite and olibin basalt sampled from Inada and Genbudo, respectively. The grain size of both rocks was under 200 mesh (<75 μm). The surface area of each rock measured by the B.E.T. method were 2.15 m^2/g for granite and 4.30 m^2/g for basalt respectively. The range of the initial concentration of Cs solution was 8.7 μg/g ∿ 95 μg/g and the weight ratio of fluid to solid was 5. The sample was enclosed in gold capsules and heated for 10 hr ∿ 1000 hr at 20°C ∿ 300°C. After heating the solutions and solids were separated by centrifugal separator. The solutions were analyzed by Atomic Absorption Spectrophotometry (AAS) and Inductively Coupled Plasma (ICP) method. And the solids were analyzed by X-ray diffraction and examined changes of mineral phases.

Result

In the case of contact time of 10 hr the weight of Cs adsorbed on basalt increased with increasing temperature and saturated from 100°C up (Fig. 1). The value of kd under condition of 300°C, 100 atm is shown in Fig. 2. As far as basalt the value of kd was more than 500 ml/g and much bigger than those of granite. And basalt showed comparatively constant value.

By the X-ray diffrection analysis it was found that Smectite was formed in the basalt under the condition of 300°C (Fig. 3, Fig. 4).

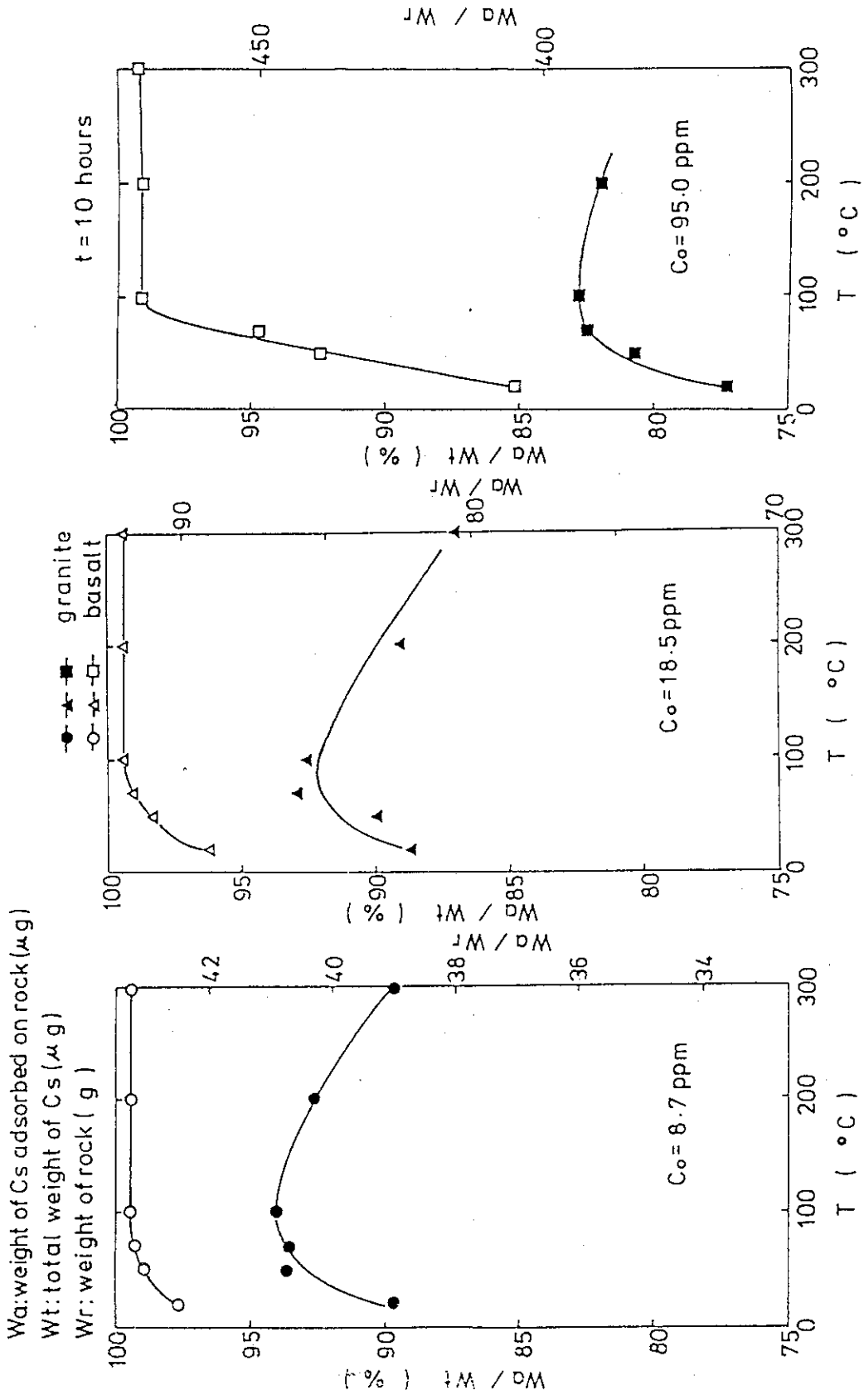

Fig.1 Influence of temperature on sorption of Cs on rocks

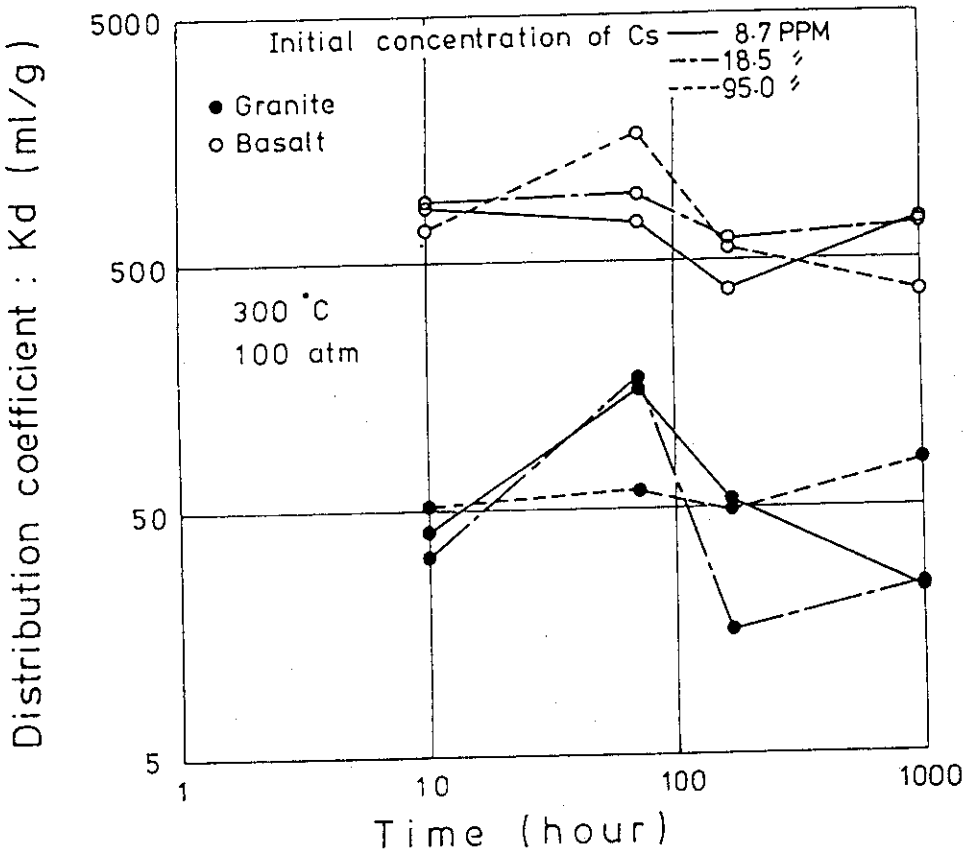

Fig.2 Influence of contact time on sorption of Cs on rocks at 300°C

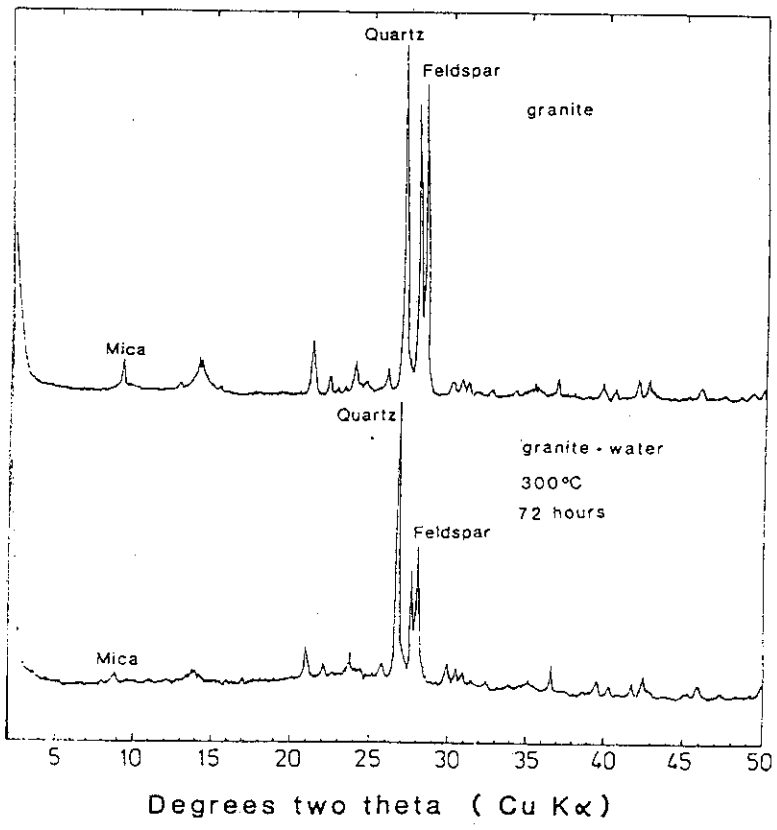

Fig.3 X-ray diffractograms of granite before and after experiments

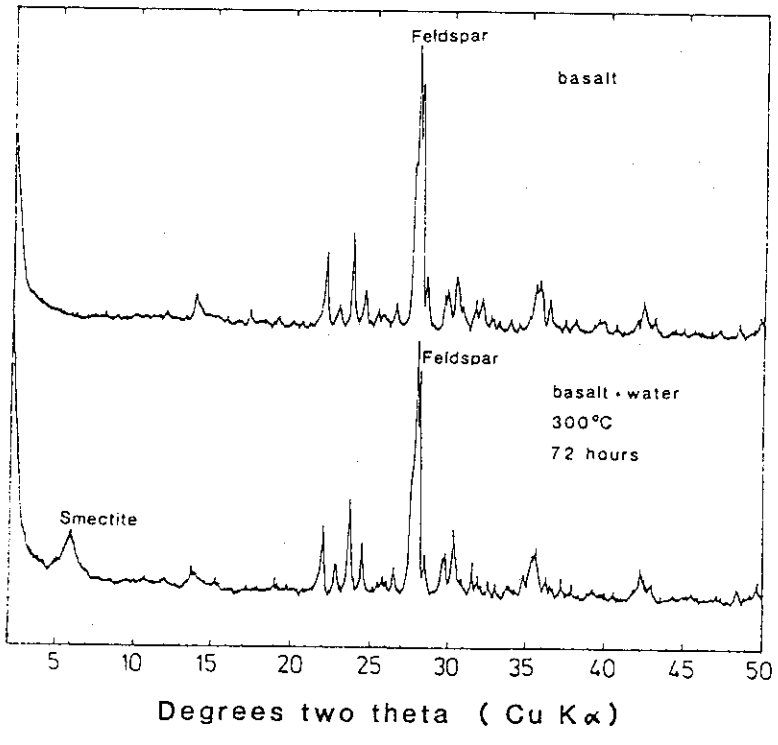

Fig.4 X-ray diffractograms of basalt before and after experiments

4.3.3 Compatibility test of near field materials under γ-ray irradiation

S. Muraoka

In assessing the long term integrity of and for designing the near field area around the engineered barrier, an understanding of the effect of irradiation on the interaction between barrier materials and their circumstance must be considered.
To data the effect has not been adequately addressed.

The present study was planed to clarify the effect of γ-ray irradiation on compatibility between rock and glass, leaching stability of glass and corrosion resistance of canister materials. During a two years period, since 1981, the study of γ-ray irradiation effect on corrosion resistance of alloys and some properties of concrete material have been carried out by use of ^{60}Co radiation source.

From this March, two series of γ-ray irradiation test have been started. One is the test by use of ^{137}Cs source of 2660 Ci and ^{90}Sr source of 14700 Ci in hot cell of WASTEF. Encapsuled specimens in stainless steel tube and uncapsuled ones were arranged around the each source as shown in Fig. 1. The combination of materials of specimens are shown in Table 1. Prior to the irradiation test, the dose rate adjacent to the source cases were measured. Dose rate of ^{137}Cs and ^{90}Sr were 6×10^6 R/h and 2.2×10^3 R/h respectively. Bentonite mixed with water was packed into the granite rock. The ratio of bentonite and water was 1.5 kg/2.5 l. In the case of ^{90}Sr test, the temperature increase due to its decay heat was measured by copper-constantan thermo-couples. In equilibrium condition, the temperatures were 74°C, 54°C and 41°C at each point measured by No.1, No.2 and No.3 thermo-couples shown in Fig. 1.

The other test has been carried out by use of spent fuel in JMTR. Specimens were encapsuled ones in the same way of ^{137}Cs and ^{90}Sr irradiation test. The γ-ray flux distribution was measured at the area of specimens as shown in Fig. 2. After 3, 6, 12 and 24 month's irradiation, solid specimens and solution are to be analyzed by XMA, TEM and ICP methods.

Table 1 The combination of specimens

No.	Specimens
1	SUS 304 - deionized water
2	SUS 309S- deionized water
3	SUS 304 - granite - granite saturated water
4	SUS 309S- basalt - basalt saturated water
5	glass - granite - granite saturated water
6	glass - basalt - basalt saturated water
7	glass - deionized water
8	SUS 304 - bentonite
9	SUS 309S - bentonite
10	glass - bentonite
11	granite - bentonite
12	basalt - bentonite

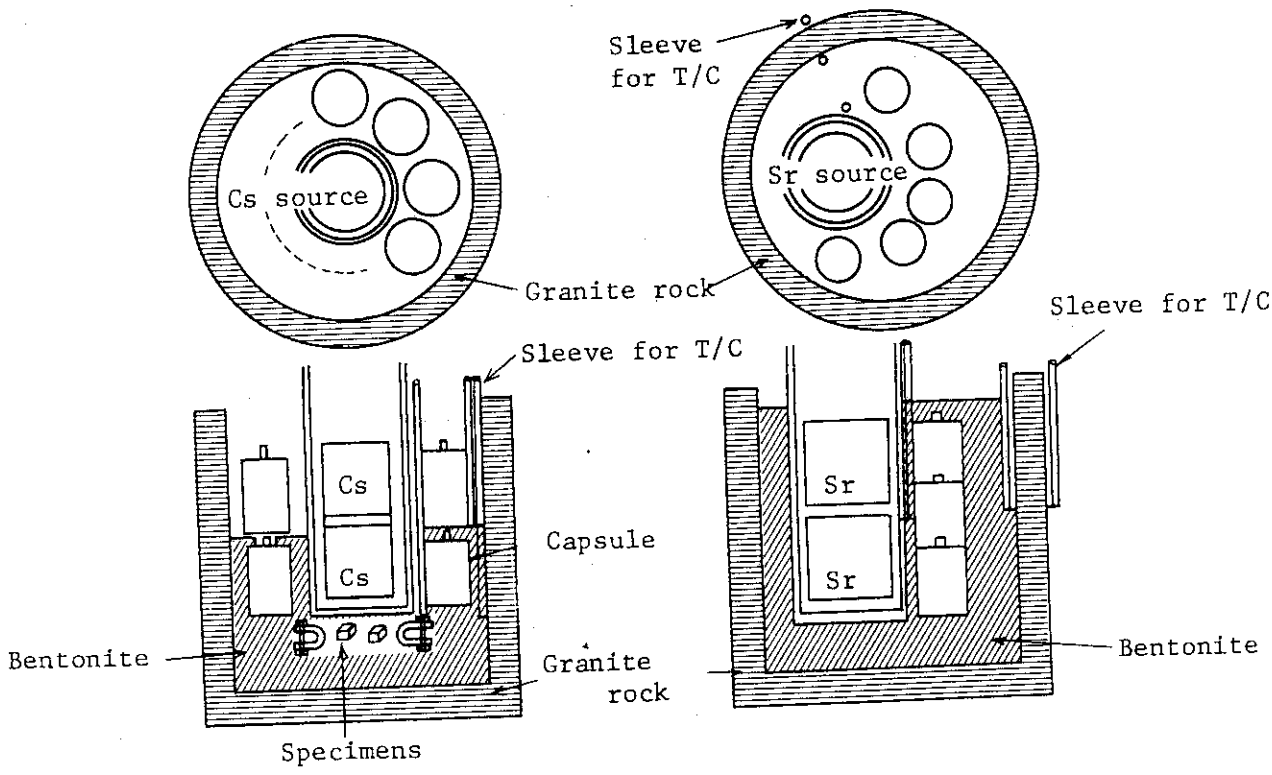

Fig. 1 Arrangement of the specimen around Cs and Sr source

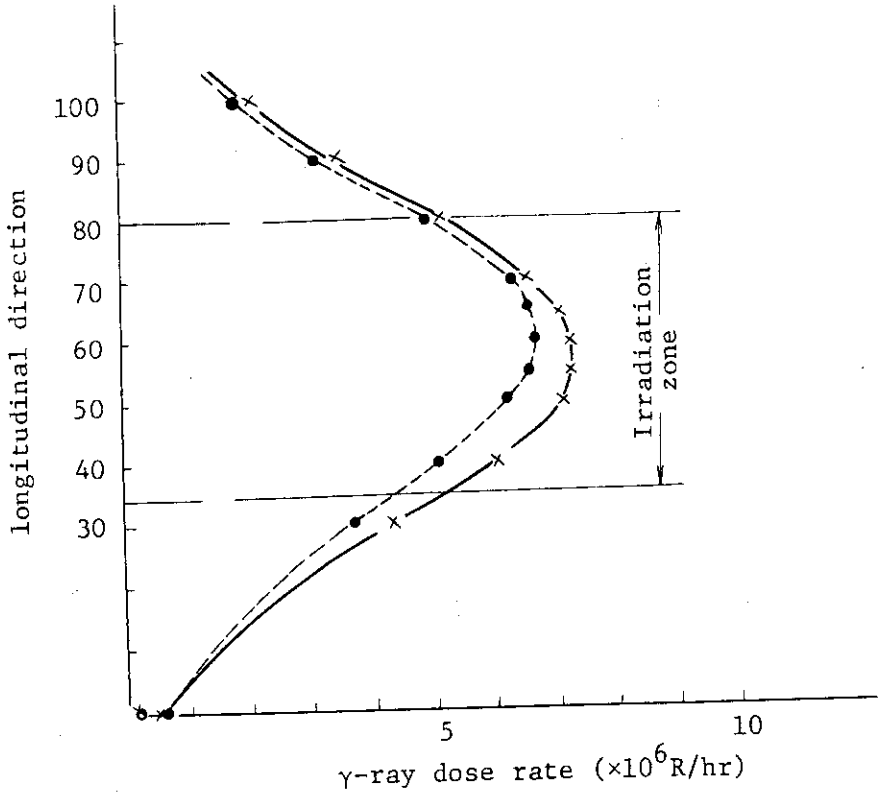

Fig. 2 γ-ray distribution in the spent fuel rack

5. Safety Study of Nuclear Facilities on Vitrified HLW's Stream

T. Takeda

One of the problems to be solved urgently is to establish safe storage and transportation of returned-vitrified HLWs. The Japanese power companies and their organized committee is conceputually designing the waste storage facilities and shipping packages. The regulatory bodies will have to study the safety of the facilities. In order to support the regulatory bodies, safety evaluation methods have been studied and a committee was held to discuss the program and results of research items. The committee consist of specialists of our institute, nuclear industries and universities. In this year, two major items have been discussed in the committee : (1) to pick up and to clarify problems on safety examination and (2) to clarify deferences between computor codes, which are used for safety assessment of reactors, and their applicabilities for safety examinations of the facilities.

As for the first, many critical points on the safety examination of the actual facilities have been generally discussed in the field of each specialist, but considerations are required to select the safety research items necessary for practical safety examination procedures. Therefore, it has been decided to continue the discussion in next year through tentatively-referential safety examination using one of typical models of realistic storage facilities and using documents materialized by a design company being proxy for future applicants. This is one of the most effective procedures to find out the critical subjects for the safety research on the HLWs storage facilities design and regulatory guides.

As for the second, preceding to the tentatively-referential safety examination, some reference problems have been selected and solved by using of some typical computer codes developed already for reactor safety for each problems. Two structural, one thermal and one shielding performances were evaluated the vitrified waste in canister and their storage facilities. For example, the first structural evaluation is to analyze thermal stress of the glass in a canister and the second one is to estimate the deformation behavior of the vitrified HLWs subjected to impacts of drop, which is analyzed by using STEALTH and newly-developed deformation analysis code using a model of combination of springs and rigid-bodies crackings and powderization. The analysis of cracking and powderization seems to be one of own problem for safety evaluation of the storage facility.

Experiments relating to behavior of glass powderization and fracturing mechanism by using WASTEF are planned in next fiscal year.

6. Characterization of waste form to be returned from over-sea reprocessing

M. Senoo, Y. Kiriyama and M. Satoh

The Japanese electric utilities have entrusted reprocessing their nuclear spent fuel to the reprocessing companies in United Kingdom and in France.

In September 1982, COGEMA, French reprocessing company, presented the specifications of the high level waste form.

In order to judge whether the waste form is acceptable or not, it is urgent to confirm characteristics shown in the presented specifications and replenish deficit data necessary for safety evaluation of storage and temperature.

JAERI has measured the characteristics of the waste form under consignment from the electric utilities.

The measured items and the used methods are following.

i) Density; Archimedes method

ii) Chemical homogeneity; X-ray fluorescence analysis

iii) Leachability; Soxhlet type; 1∿7 days
; ISO type; 149 days

iv) Thermal conductivity; Transit heat flow measuring method

v) Transient temperature; Differential Scanning Calorimeter(DSC) and Thermo-mechanical Analysis (TMA)
Softening temperature; DSC and TMA
Devitrification temperature; DSC

vi) Viscosity; Rotating cylinder viscometry

vii) Thermal expansion coefficient; TMA

viii) Mechanical properties; One axial press strength, tensile strength and bending strength using Instron type apparatus.

ix) Thermal-shock resistance; Dropping into water

x) Irradiation test; Preliminary test for α damage irradiated by thermal neutrons of up to 1.1×10^{18} n/cm^3

xi) Determination of chemical composition ; X-ray fluorescence analysis

In general, the results obtained from the measurements are in good accord with COGEMA's Data shown in 1982.

7. Preparation and hot operation of WASTEF

S. Tashiro

7.1 Activities in the year

The Waste Safety Testing Facility (WASTEF) was completed in Summer of 1981 in order to obtain useful data for the safety assessment of high level waste management by testing the solidified form and relating materials. Figure 1 shows the first floor plan of the facility and Table 1 lists the capacity of the cells to handle radioactive materials. After the completion, preparation and performance tests of the each apparatus and equipment were continued at the cold stage. Main items performed in the year are listed in Table 2.

During the cold stage the thermal conductivity and leachability of a vitrified form were measured which is expected to be returned from the oversea reprocessing project.

7.2 Production of vitrified test samples

Four liters of vitrified products were made by four runs of vitrification (1 liter each) as starting up of the hot operation. The flow sheet of vitrification apparatus is shown in Fig. 2.

In the beginning four years of the hot operation of WASTEF, synthetic wastes which contain one or some radioactive nuclide are used so that more accurate and wider ranges of data will be accumulated than cold simulated or actual wastes. The heating program of the melter was, therefore, arranged according to the purpose as shown in Figure 3. The heating system of the melter has five components that are top (TRC-11), middle (TRC-12), bottom (TRC-13), freeze valve (TRC-14), and annealing (TRC-15). Vitrified products are taken out through freeze valve into canister in annealing furnace after melting at 1200°C for 2 hours. A brief description about the four rans performed this year is listed in Table 3.

7.3 γ-Scanning test of vitrified products

The measurement of homogeneity of radioactive materials in the vitrified products is essential to obtain accurate data for the safety assessment.

For this purpose a γ-scanning apparatus was installed in No. 1 cell. It has De-detection with three kinds of collimators that are 0.3 mm, 0.5 mm

and 1 mm in diameter, and a measuring stage which can rotate samples of max. 5 ℓ block to every direction (cf. Figure 4).

Figure 5 shows the data obtained from three directions of 1 ℓ product in stainless steel canister of 80 mm in diameter, 250 mm in length and 5 mm in thickness.

7.4 Preparation of testing equipments

Main apparatus and equipments installed in the cells of WASTEF are listed in Table 4. These equipments are at the moment completed for hot operation after repetition of the cold performance tests and improvements.

7.5 Future plan

In the next fiscal year the following items are planned to be tested; gaseous concentrations of volatile elements in a storage canister (Cs-134 etc.), dispersion in air of fine granules of vitrified product (Mo-99), leachability of Neptunium (Np-237), irradiated behavior of near field materials (Cs-137, Sr-90) and α-damage behavior of vitrified forms (Cm-244, Pu-239).

These items include tests for characterization of the vitrified forms to be returned from the oversea reprocessing.

After using radioisotopes such as Cs-137 for the beginning four years, test using actual wastes is planned to start in 1986.

Table 1 Maximum capacity of the facility for radioactive material handling

Cell	βγ-emitter or actual waste	αγ-emitter
No. 1	5×10^4 Ci (1×10^6 Ci in storage)	—
No. 2	5×10^4 Ci	—
No. 3	5×10^4 Ci	—
No. 4	1×10^4 Ci	200
No. 5	5×10^2 Ci	200
Pb	20	10

Table 2 Main activity in the year

Date	Item
27, Oct., '82	Receiving the certification for radioisotope handling
12, Oct. ~ 13, Nov.	All through cold performance tests
15, Nov.	Receiving the certification for fissile material handling
22, Nov.	Setting up control area in the facility
1, Dec.	First hot run of vitrification
14, Dec.	Second hot run of vitrification
18, Jan., '83	Third hot run of vitrification
22, Feb.	Fourth hot run of vitrification
28, Feb.	Starting nearfield simulation test with a 10^4 Ci of Cs-137 and Sr-90

Table 3 Specification of vitrification

Run No.	Composition of product			Weight of product (g)	Checking items
	Matrix	Waste (Content, %)	RI (Activity, mCi)		
H82001	JAERI	JW-C(12)	Cs-137(0.16)	3054.8	Contamination of the apparatus & cell Performance of off-gas system Waste generation
H82002	JAERI	JW-C(12)	Cs-137(12.8)	2848.8	
H82003	JAERI	JW-C(12)	Cs-137(15.4)	3052	
H82004	COGEMA	JW-C(17.5)	Cs-137(15.9)	2722.5	COGEMA Spec. Carbon pot.

Table 4 List of testing equipments installed in the cells

Cell No.	Installed equipment
No. 1	γ-Scanning apparatus Storage test apparatus (test equipment for heat generation, temperature distribution, cooling and evaporation)
No. 2	Vitrification apparatus (systems for pre-treatment of waste, vitrification and off-gas treatment)
No. 3	Disposal test apparatus Sample preparation apparatus (machines for cutting, core-drilling, polishing, crashing and shieving)
No. 4	Characterization test apparatus (measuring equipments for heat generation, thermal conductivity, leachability, sample dimension and density)
No. 5	α-Damage test apparatus (remelting furnace, cutting and polishing machine, herium detector and DSC)
Pb	Microscope Micro γ-scanning apparatus

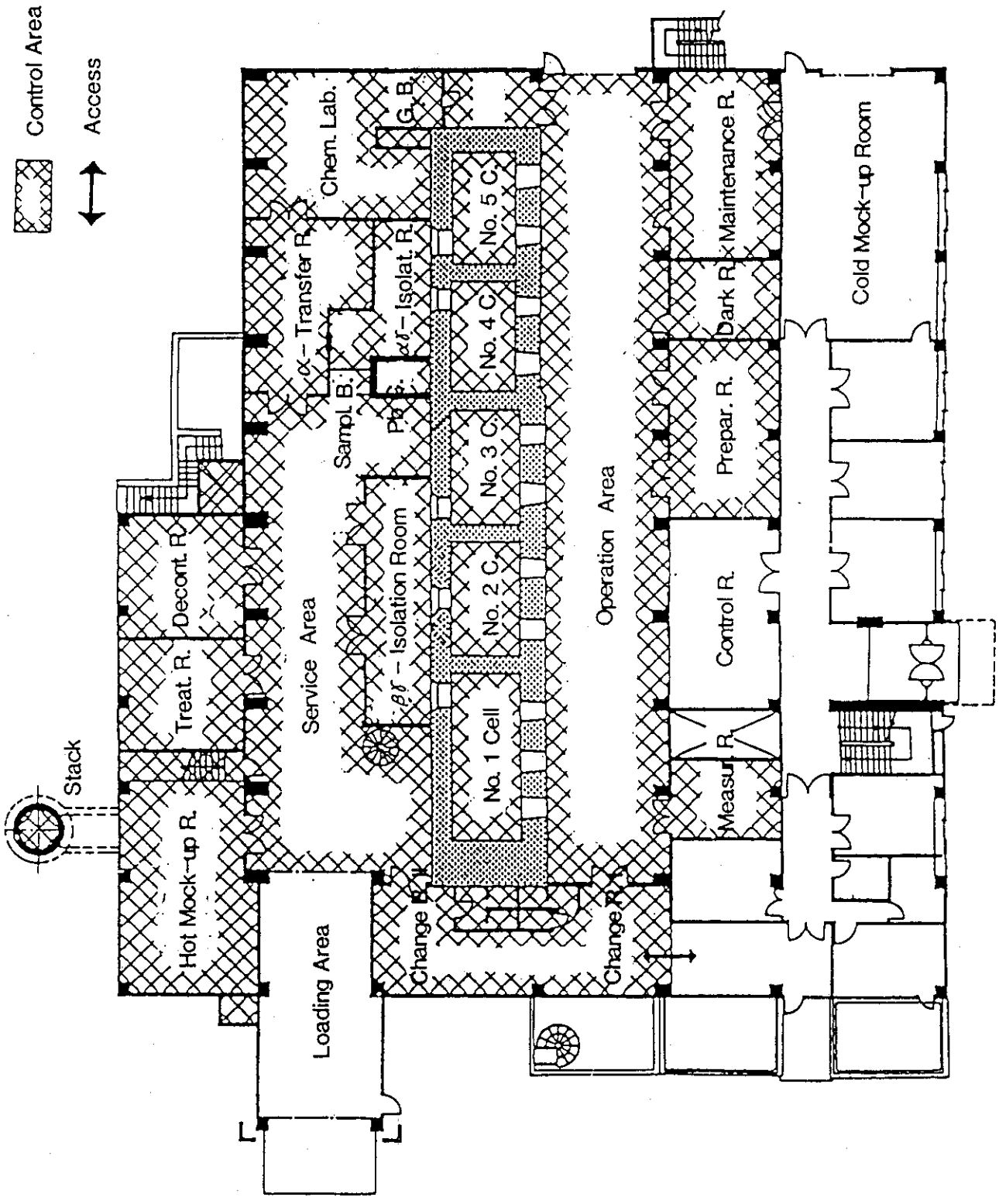

Fig. 1 First floor plan of WASTEF

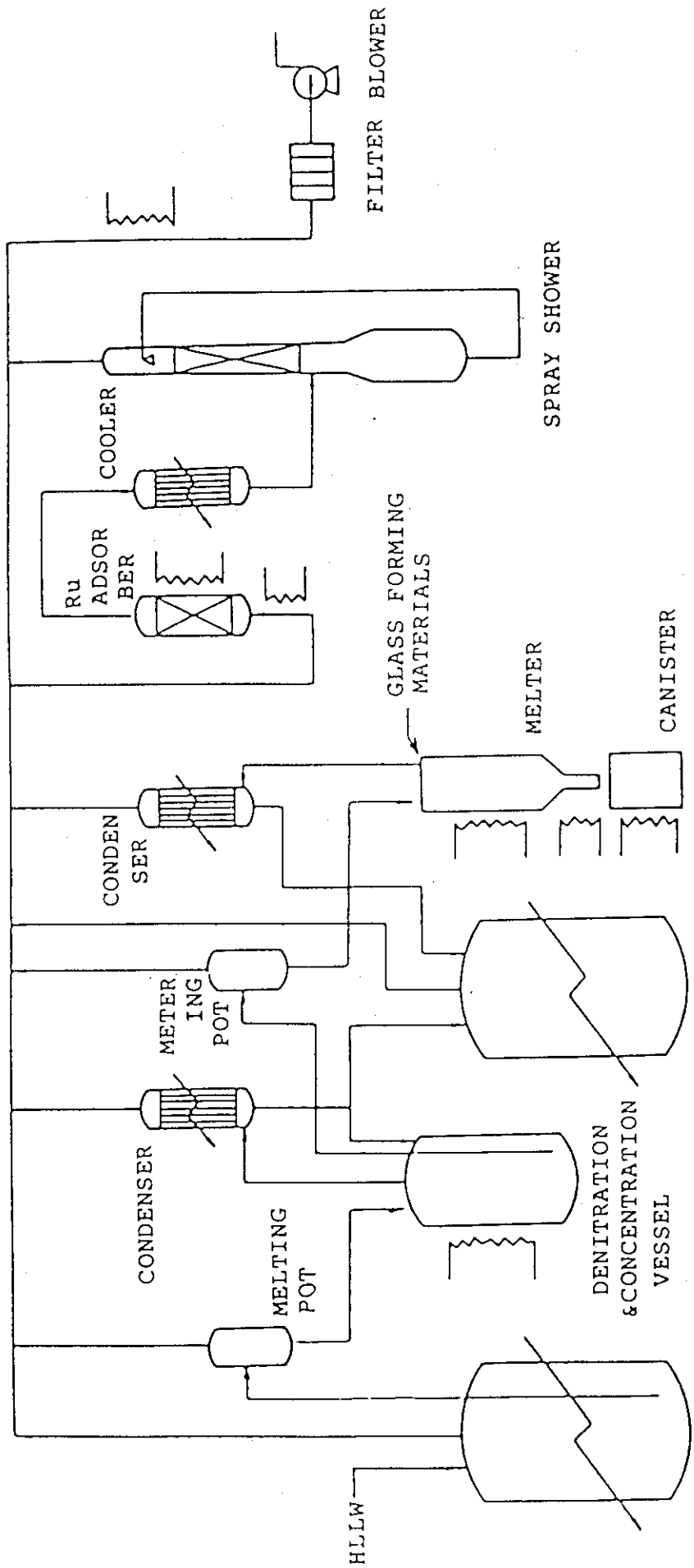

Fig. 2 Flow sheet of vitrification apparatus

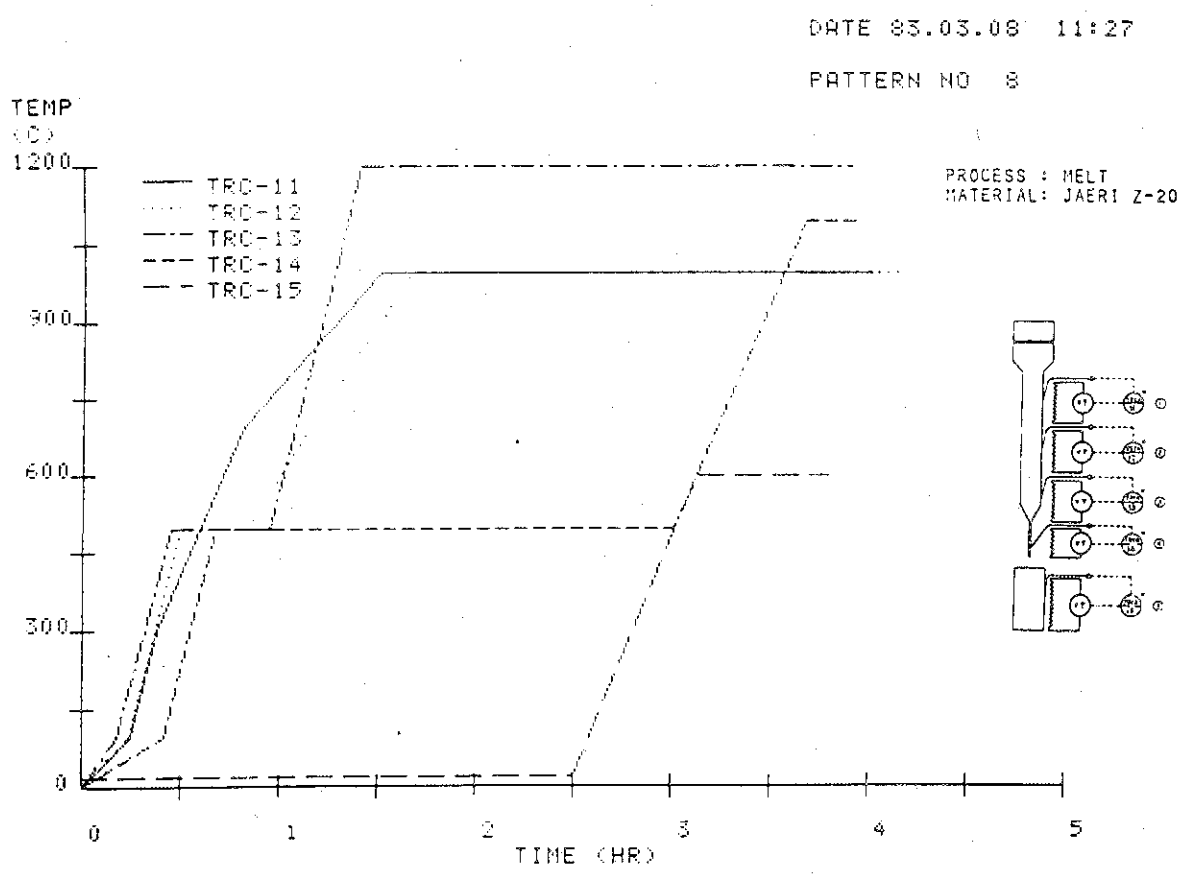

Fig. 3 Heating pattern of vitrification

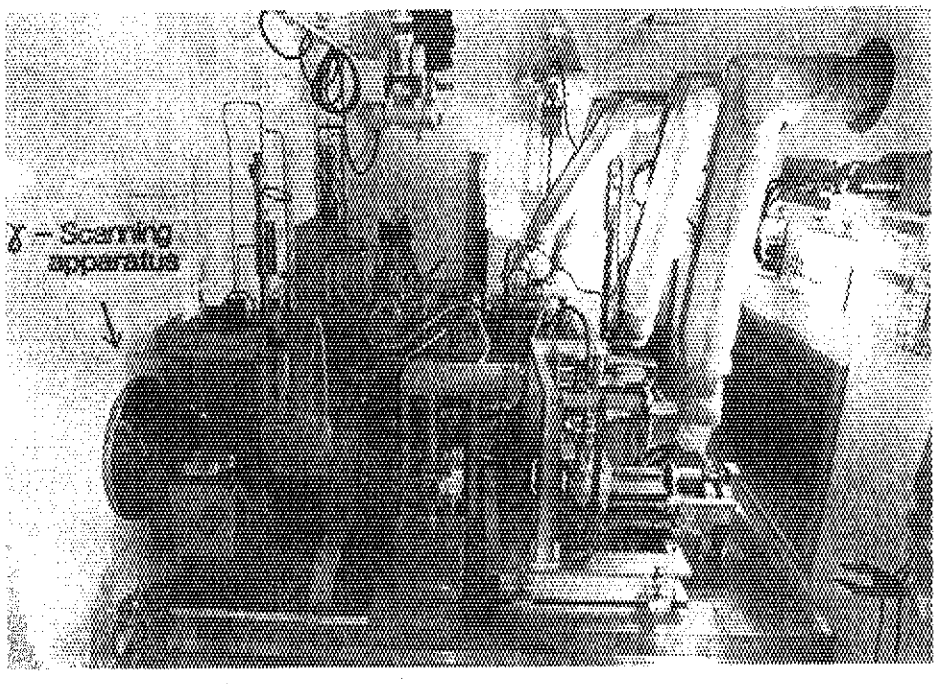

Fig. 4 Photograph of No. 1 cell

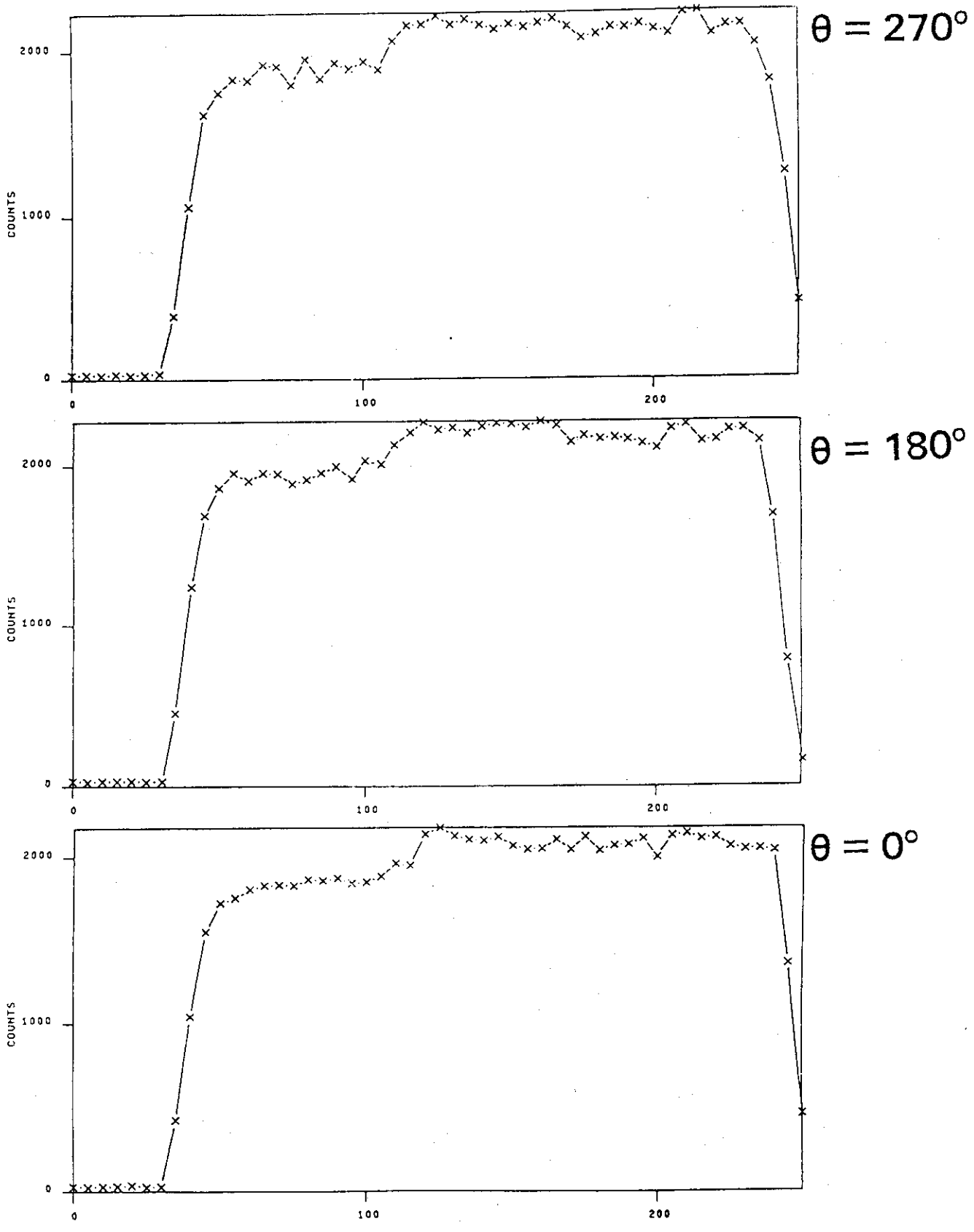

Fig. 5 Result obtained by γ-scanning